International Journal of Thermofluids 23 (2024) 100786

Contents lists available at ScienceDirect

International Journal of Thermofluids

journal homepage: www.sciencedirect.com/journal/international-journal-of-thermofluids

Two-phase analysis of heat transfer of nanofluid flow in a wavy channel heat exchanger: A numerical approach

Mohammad N. Fares [a], Mohammad AL-Saad [b], Heider H.J. Almutter [a], Dheyaa J. Jasim [c], Mohammad Ali Fazilati [d,e,*], Soheil Salahshour [f,g,h], Sh. Baghaei [i]

[a] Department of Chemical Engineering, Faculty of Engineering, University of Basrah, Basrah, Iraq
[b] Department of Mechanical Engineering, Faculty of Engineering, University of Basrah, Basrah, Iraq
[c] Department of Petroleum Engineering, Al-Amarah University College, Maysan, Iraq
[d] Efficiency and Smartization of Energy Systems Research Center, Khomeinishahr Branch, Islamic Azad University, Isfahan, Iran
[e] Stone Research Center, Khomeinishahr Branch, Islamic Azad University, Isfahan, Iran
[f] Faculty of Engineering and Natural Sciences, Istanbul Okan University, Istanbul, Turkey
[g] Faculty of Engineering and Natural Sciences, Bahcesehir University, Istanbul, Turkey
[h] Department of Computer Science and Mathematics, Lebanese American University, Beirut, Lebanon
[i] Department of Mechanical Engineering, Khomeinishahr branch, Islamic Azad University, Khomeinishahr, Iran

ARTICLE INFO

Keywords:
Two-phase analysis
Nanofluid flow
Wavy channel heat exchanger

ABSTRACT

The heat transfer improvement by using *CuO*/water nanofluid (*NF*) in a wavy channel is evaluated numerically using the turbulent two-phase mixture and theκ-ε models. The numerical work is a 2-dimensional model created and analyzed in Gambit and Ansys Fluent software, respectively. The flow Reynolds (*Re*) numbers of 8000 – 40,000, wavelength ranging from 0 – 0.4 m, and solid volume fraction (*SVF*) of 0 % to 4 % are investigated. In all cases, a constant heat flux of q''=5000 W/m^2 is applied on the outer surface of the heat exchanger. The heat transfer and fluid flow were analyzed by the flow visualization method and heat transfer evaluation indexes. The results show that by increasing the *Re* number, the vortices increase and more turbulence are generated in the vicinity of the waves near the channel inlet. As the amplitude of the channel waves increased, the velocity at the top of the wave increased, and the resulting pressure gradient behind the wave is intensified and the reverse flow is generated. The improving effect of using *NF* is more prominent where the effect of other enhancing factors is weak. For wall amplitude of 0.1 m, by increasing the *SVF* from 1 – 4 % the average *Nu* number (Nu_{avg}) increased by 35 % and 22 % in *Re* = 8,000 and 40,000, respectively.

1. Introduction

Industrial development relies heavily on the application of heat exchangers, and considering their large application in industries the study of their heat transfer improvement is a live subject. The heat transfer improvement could be made via both active and/or passive ways; Despite the problems of active methods, by their large benefits the passive techniques are the most popular and have drawn large attention through the years [1]; increasing the contact surface using the fins [2–4], employing the baffles [5–7] or vortex generators [8–13], inside the fluid flow channel and application of metallic porous foams are some of the most popular techniques. The application of porous materials extends the heat transfer area and increases the heat transfer rate [14]. The large area per unit volume of porous materials (such as metal foams) has made them a good candidate for heat transfer enhancement. The application of porous materials beside the phase change materials (*PCMs*) makes use of both the heat storage and heat transfer potential simultaneously [15]. Among passive techniques, methods based on the deformation of the channel wall draw large attention; using the waveforms and corrugation on the wall for heat transfer improvement has been considered by many researchers [16–18]. The heat transfer enhancement resulting from the wall deformation is due to the increased mixing, the vortices, and rotational motion. When fluid flows through a corrugated channel, the flow is disturbed due to the growth of rotational areas close to the corrugated wall, which finally improves heat transfer [19]. Corrugated walls improve heat transfer by eliminating or reducing the thickness of the thermal boundary layer and increasing the flow mixing [20]. The waveform of the wall would enhance the transverse flows in the channel and therefore increase the heat transfer rate [21]. It

* Corresponding author.
E-mail address: fazilati@iaukhsh.ac.ir (M.A. Fazilati).

https://doi.org/10.1016/j.ijft.2024.100786

Available online 30 July 2024

Nomenclature

Abbreviation

LHS	latent heat storage
NF	nanofluid
NP	nanoparticle
PCM	phase change material
PT	plain tube
QUICK	quadratic upstream interpolation for convective kinetics differencing scheme
SIMPLE	semi-implicit method for pressure-linked equations
SVF	solid volume fraction (%)

Symbols

a	amplitude (m)
c_p	specific heat (kJ/kg.K)
CuO	copper oxide
Da	Darcy number
f	friction factor
g	gravity acceleration (m/s^2)
G	mass flow rate (kg/s)
h	local convective heat transfer coefficient (W/m^2. K)
J	heat transfer efficiency
k	thermal conductivity (W/m.K)
L	length (m)
Nu	Nusselt number
Pr	Prantdl number
q''	heat flux (W/m^2)
Ri	Richardson number
Re	Reynolds number
S	surface function (m)
T	temperature (K)
u, v	velocity components (m/s)
U,V	velocity (m/s)
w	width (m)
x	channel length (m)
Y	channel height (m)

Greek symbols

α	wave amplitude
Δ	difference
ε	turbulent dissipated energy
φ	nanofluid concentration (%)
κ	turbulent kinetic energy
λ	wavelength
μ	dynamin viscosity (Pa.s)
ρ	density (kg/m3)
τ	tension (Pa)

Subscripts

avg	average value
b	bulk
f	base fluid
e	entrance region
eff	effective
h	hydraulic
i, in	inlet flow
m	mixture
nf	nanofluid
p	particle
pf	particle-base fluid
s	smooth
t	turbulence
w	wall

should be noted that the heat transfer improvement is alongside the pressure drop increment. Numerical solvers are commonly used to calculate the pressure drop and heat transfer rate in corrugated channels [22–25]. Sui et al. [26] investigated the rate of heat transfer in a three-dimensional sinusoidal channel with a rectangular cross-section and water as the working fluid in a laminar flow regime. The results show that by passing the fluid through the curves in the channel, a symmetrical steady flow or Dean vortices is generated. Ferley and Ormiston [27] compared heat transfer in channels with sinusoidal walls in elliptical and v-shaped cross sections in the laminar flow regime. The results demonstrated that in terms of friction factor, heat transfer rate and Nu_{avg}, the sinusoidal wall channel performs better. Considering that increasing the heat transfer rate on one hand and decreasing the rate of pressure drop on the other hand in corrugated ducts are two desirable, albeit opposite goals, efforts were made to optimize the wall shape of these ducts [28]. As an important characteristic of internal flows, the entrance length takes effect from the wavy region. Mehta et al. [29] analyzed the hydrothermal properties of the laminar forced flow of water inside the wavy channel with different types of constant, increasing and decreasing amplitudes at different *Re* numbers and amplitude slopes (A). They found the independency of *Nu* number from the channel geometry at low *Re* and *A* numbers. As the other heat transfer improving factor, nanofluids (*NFs*) found wide application in heat exchangers [30] and solar systems [31]. Several reviews demonstrate the aspects of convective heat transfer improvement made by using *NFs* in different geometries [32,33]. Compared to other improving methods, *NFs* could be used as an inexpensive method to enlarge the heat transfer area and improve heat transfer. The *NF* flow as a two-phase medium could be modeled using two different approaches: single-phase and two-phase. The two-phase models were studied and their aspects for modeling of *NF* flow have been investigated in different studies [34,35]. The two-phase mixture has predicted successfully the performance of *NFs* with solid volume fraction (*SVF*) < 10 % with the highest accuracy [19]. Hejazian [36] demonstrates that for the simulation of turbulent forced convection *NF* flow with *SVF* < 1 %, the results of two-phase modeling are more accurate than that of single-phase models. Dormhommadi et al. [37] built a numerical model to compute the entropy generation rate in a sinusoidal wavy-wall channel with the *NF* of *Cu*-water as the heat transfer fluid. The effects of *SVF*, Richardson (*Ri*) number, wave amplitude number and wavelength were studied. The showed optimal wave amplitude ratio is, for wavelengths 1 and 2. Nazari et al. [37] studied the heat transfer of water- *CuO NF* in a channel with a porous media in different *Re* and Darcy (*Da*) numbers. The results demonstrated the heat transfer improving effect of employing porous medium and *NF*. Kumar et al. [38] studied the thermo-flow behavior of non-Newtonian *NF* which flows inside the trapezoidal wavy channel. They reported the *Nu* number, pressure drop, and performance factor for different *SVF* values, *Pr* and *Re* numbers. They reported the growth of *Nu* number and pressure drop and reduction of performance factor by increasing the *SVF, Re* and *Pr* numbers. To improve thermal management in electronic systems, Mahsa Hajialibabaei et al. [39] designed a novel wavy channel heat sink. To achieve better flow mixing and uniform temperature distribution, their design employed secondary branches with gradually decreasing spacing and height. They investigated the effect of flow rates on heat sink temperature and found that a 90-degree branch angle with a 1 mm width results to 5.27 % temperature reduction compared to the basic wavy channel heat sinks. To the best of the authors' knowledge and through the literature review, it was found that the two-phase turbulent flow of water/*CuO* inside the wavy channel has not been investigated yet. In the present study, the turbulent

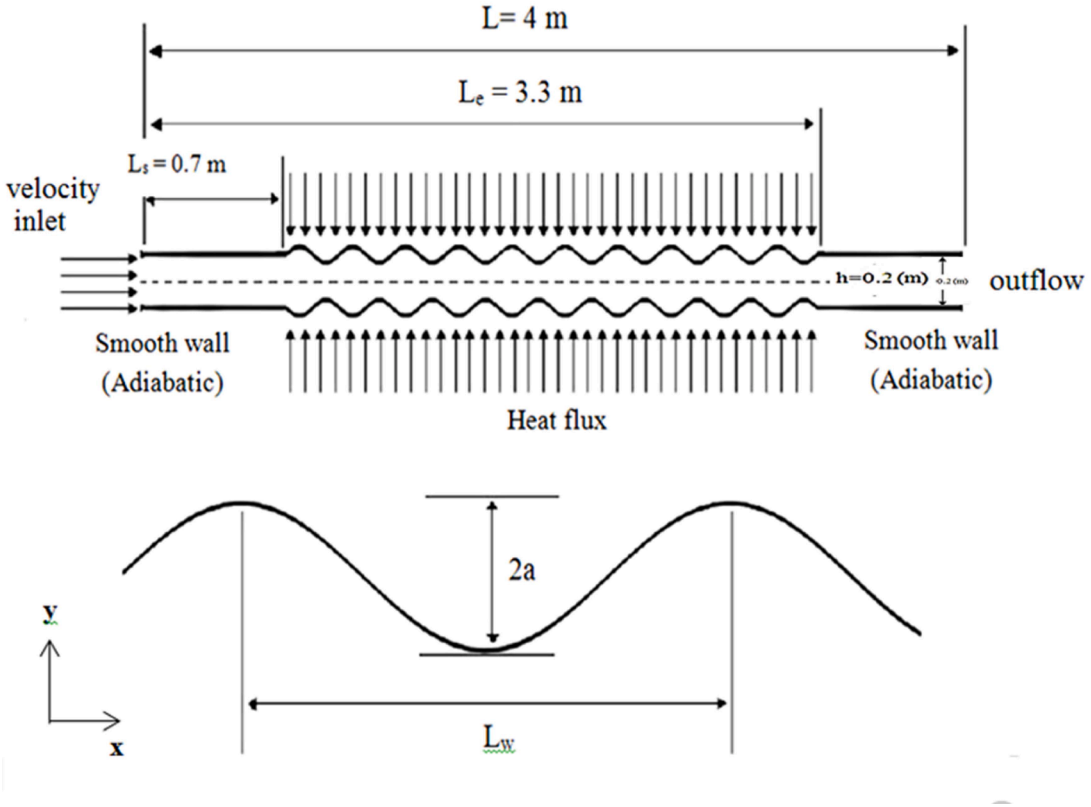

Fig. 1. The geometry of the problem, the boundary conditions and dimensions.

Table 1
Thermophysical properties of the base fluid and *CuO* nanoparticles [40].

	water	*CuO*
ρ (kg/m^3)	998	6350
C_p (J/kgK)	4182	535.6
k (W/m.K)	0.597	69
μ (kg/m.s)	0.000993	–
Nanoparticle size (nm)	–	100

Table 2
Thermophysical properties of *NF* at different *SVF*s.

SVF	ρ_{nf}(kg/m^3)	C_{nf}(J/kg.K)	k_{nf}(W/m.K)	μ_{nf}(kg/m.s)
%1	1053.2	3956.87	0.62975	0.00108856
%2	1108.3	3753.74	0.646807	0.0011987856
%3	1163.254	3570.3	0.66418088	0.0013336891
%4	1218.272	3404.24	0.6818802	0.001492664

flow and heat transfer of the *CuO*-water *NF* in a corrugated channel is investigated. The outer wall of the channel is subjected to constant heat flux and the fluid flow is fully developed. The sensitivity analysis is made to reveal the effect of *Re* number and *SVF* on heat transfer of fluid flow. To model the fluid flow, the turbulent two-phase mixture and theκ-ε models are considered. In the next section, the problem and the governing equations are described. After explaining the numerical procedures, the results are presented by discussing the diagrams and finally, the conclusions are drawn.

2. Problem description

Fig. 1 shows the geometry of the studied problem; also, the details of the wall can be seen. The fluid flow is between two corrugated sinusoidal plates with a total length of L and an inner width of h between the two plates. The form of wall corrugation is according to Eq. (1). To achieve the fully developed condition, a smooth adiabatic length (L_s) is considered at the inlet of the channel; also, the outer wall is subjected to a fixed heat flux of 5000 W/m^2.

$$S = \pm \frac{w}{2} \pm \text{asin}\left[\frac{2\pi\,(x - L_s)}{L_w}\right] \quad L_s \le x \le L_e \tag{1}$$

The base fluid and nanoparticle (*NP*) are water and *CuO*, respectively whose properties are listed in Table 1 [40]. The fluid flow is assumed incompressible, two dimensional, two-phase and axisymmetric. The previous studies reveal that the *NF* could exhibit both Newtonian and/or non-Newtonian behavior; however, in this work, the *NF* flow is considered Newtonian. The *Re* number is between 8000 and 40,000 and the fluid flow is turbulent. The *SVF* is 0%, 1%, 2%, 3% and 4% and the wall wavelengths are 0, 0.1, 0.2, 0.3 and 0.4 m. The length of the annulus is 4 m with its corrugated part of 2.5 m; also, the inlet temperature is 293 K.

2.1. Governing equations

The *NF* flow is considered steady and incompressible and the effect of viscose dissipation is neglected. The flow behaves Newtonian and its properties are assumed to be independent of the temperature. In addition, the relative velocity between the nanoparticles and base fluid is ignored. The equations of continuity, momentum and energy for the two-phase mixture model can be expressed as Eqs (2) – (5) [41]. In the following equations, the subscripts "*m*", "*f*" and "*p*" stand for the mixture, base fluid and nanoparticles, respectively; also φ_k is the *SVF* of phase *k*.

$$\vec{\nabla}.\left(\rho_m.\vec{V}_m\right) = 0 \tag{2}$$

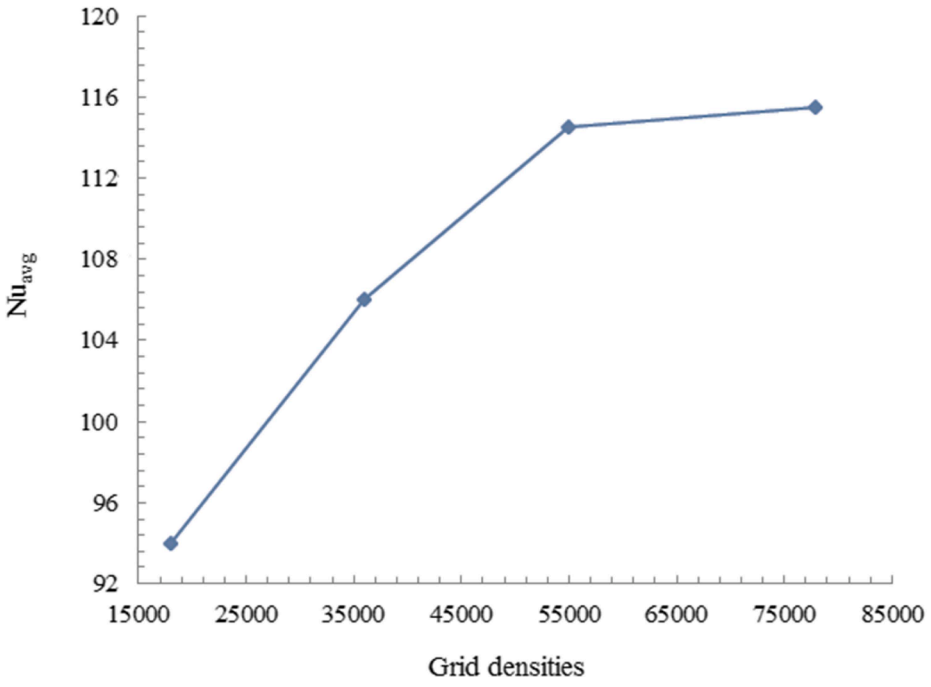

Fig. 2. The variation of Nu_{ave} for different grid densities.

Table 3
The Nu_{ave} for different grid sizes and the percent change at each step.

Mesh size	Nu_{avg}	Percent change
60 × 300	94	–
80 × 450	106	12.80%
550 × 100	114.5	8.00%
650 × 120	115.5	0.87%

$$\vec{\nabla}.\left(\rho_m \overrightarrow{V}_m \overrightarrow{V}_m\right) = -\vec{\nabla}P_m + \vec{\nabla}\left(\left(\mu_m + \mu_{t,m}\right)\nabla.\vec{V}_m\right) + \vec{\nabla}.\left[\sum_k \varphi_k \rho_k \overrightarrow{V}_{dr,k} \overrightarrow{V}_{dr,k}\right] \tag{3}$$

$$\vec{\nabla}.\left[\sum_k C_{pk}\varphi_k \vec{V}_k T\right] = \vec{\nabla}.\left(k_{eff}\vec{\nabla}T\right) \tag{4}$$

$$\vec{\nabla}.\left(\varphi_p \rho_p \vec{V}_m\right) = \vec{\nabla}.\left(\varphi_p \rho_p \vec{V}_{dr,p}\right) \tag{5}$$

The mixture properties including density, viscosity, specific heat, thermal conductivity and mass average and drift velocities are defined in Eqs. (6) – (11) [41],

$$\rho_m = \sum_k \varphi_k \rho_k = (1-\varphi)\rho_f + \varphi\rho_p \tag{6}$$

$$\mu_m = \sum_k \varphi_k \mu_k = (1-\varphi)\mu_f + \varphi\mu_p \tag{7}$$

$$(\rho C_P)_m = (1-\varphi)(\rho C_P)_f + \varphi(\rho C_P)_p \tag{8}$$

$$k_{eff} = k_f\left[\frac{k_p + 2k_f - 2\varphi(k_f - k_p)}{k_p + 2k_f + \varphi(k_f - k_p)}\right] \tag{9}$$

$$\overrightarrow{V}_m = \frac{\sum_{k=1}^{n}\varphi_k\rho_k\overrightarrow{V}_k}{\rho_m} = \sum_{k=1}^{n} x_k \overrightarrow{V}_k \tag{10}$$

$$\overrightarrow{V}_{dr,k} = \overrightarrow{V}_{pf} - \overrightarrow{V}_m \tag{11}$$

In Eq. (10), x_k is determined using Eq. (12);

$$x_k = \frac{\varphi_k \rho_k}{\rho_m} \tag{12}$$

From Eqs (6) – (9) and the base and *NP* properties as given in Table 1, the *NF* properties in different *SVF*s could be determined which are listed in Table 2.

The relative velocity between the base fluid and nanoparticle is given

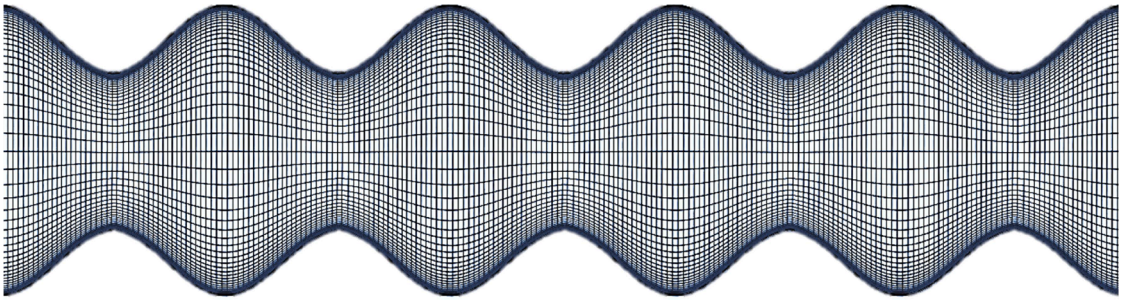

Fig. 3. A view of the employed mesh.

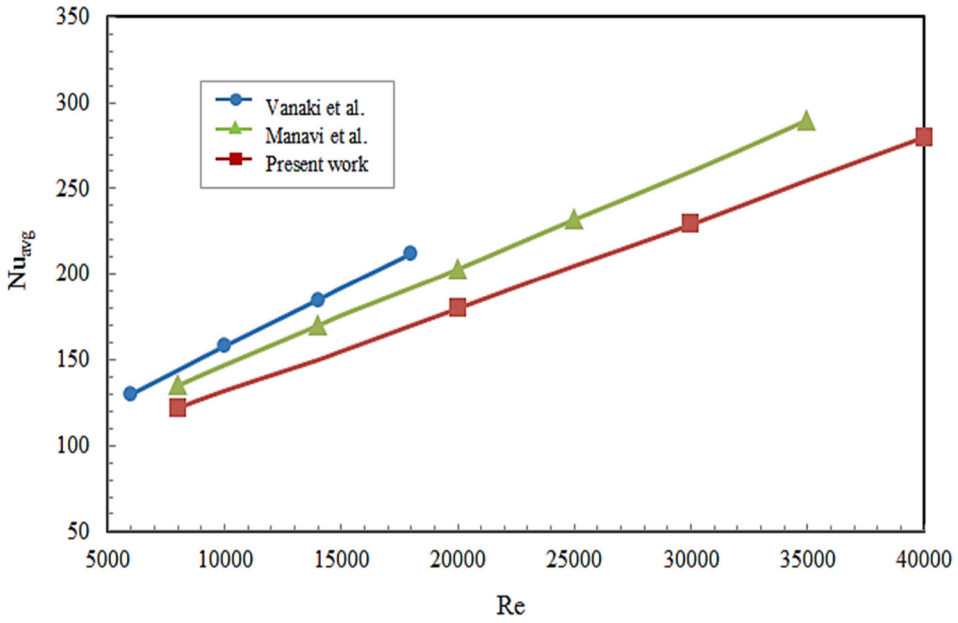

Fig. 4. The comparison of Nu_{avg} with that of Vanaki et al. [23] and Manavi et al. [44].

by Eq. (13) [42].

$$\overrightarrow{V}_{pf} = \overrightarrow{V}_p - \overrightarrow{V}_f = \frac{\rho_p d_p^2}{18\mu_f f_{drag}} \frac{(\rho_p - \rho_m)}{\rho_p} (g - (V_m.\overrightarrow{\nabla})V_m) \tag{13}$$

The drag coefficient (f_{drag}) is specified by Eq. (14),

$$f_{drag} = \begin{cases} 1 + 0.15Re_p^{0.687} & Re_p \le 1000 \\ 0.0183 & Re_p > 1000 \end{cases} \tag{14}$$

In this study, the κ-ε turbulent model is used in which the rate of turbulent dissipation (ε) and turbulent kinetic energy (κ) equations are expressed as Eqs. (15) and (16), respectively [43];

$$\nabla.\left(\rho_m \overrightarrow{V}_m \kappa\right) = div\left(\frac{\mu_{t,m}}{\sigma_k}\nabla\kappa\right) + G_{\kappa,m} - \rho_m\varepsilon \tag{15}$$

$$\nabla.\left(\rho_m \overrightarrow{V}_m \varepsilon\right) = \nabla.\left\{\frac{\mu_{t,m}}{\sigma_\varepsilon}\nabla\varepsilon\right\} + C_1\left(\frac{\varepsilon}{\kappa}\right)G_{k,m} - C_2\rho_m\left(\frac{\varepsilon^2}{\kappa}\right) \tag{16}$$

where $\overrightarrow{V}_m$ is the time-averaged velocity of the fluid. The eddy viscosity $\mu_{t,m}$ and the rate of turbulent kinetic energy generation $G_{k,m}$were modeled by Eqs (17) and (18), respectively;

$$\mu_{t,m} = \frac{\rho c_\mu \kappa^2}{\varepsilon} \tag{17}$$

$$G_{k,m} = \mu_{t,m}(\nabla V_m + (\nabla V_m)^T \tag{18}$$

In the above equations, C_1, C_2, C_μ, σ_k and σ_ε are empirical constants whose values are given below [43];

$$C_1 = 1.44,\ C_2 = 1.92,\ C_\mu = 0.09,\ \sigma_k = 1.0,\ \sigma_\varepsilon = 1.3 \tag{19}$$

2.2. Boundary conditions

The governing equations are solved in conjunction with the following boundary conditions:

- On the wall boundaries, the velocity condition of no slip and the thermal condition of constant heat flux are exerted;

$$y = mx + \alpha\sin(x/y) \Rightarrow q''(x,y) = q'',\ u = v = 0 \tag{20}$$

- The velocity and temperature at the inlet are known;

$$x = 0 \Rightarrow T = T_{in},\ u = u_{in} \tag{21}$$

- At the outlet of the channel the fully developed conditions are applied;

$$x = L \Rightarrow \frac{\partial T}{\partial x} = 0,\ \frac{\partial u}{\partial x} = 0 \tag{22}$$

- The outflow boundary condition is exerted at the exit section.

2.3. Heat transfer and fluid flow evaluation indexes

To characterize the heat transfer rate from the inner wall to the flowing *NF*, the local convective heat transfer coefficient (h) is expressed as Eq. (23) [40].

$$h(x) = \frac{q''}{T_{w,x} - T_{b,x}} \tag{23}$$

In Eq. (23), $T_{w,x}$ and $T_{b,x}$ are the wall and fluid bulk temperatures, respectively. The average heat transfer coefficient ($\overline{h}$) is determined by integration of the local heat transfer coefficient along the heated length L as given by Eq. (24) [40]:

$$\overline{h} = \int_0^L h(x)dx \tag{24}$$

Having the average heat transfer coefficient, the Nu_{avg} over the channel surface is determined based on the hydraulic diameter (D_h) and the k_{eff}, according to Eq. (25) [40],

$$Nu_{ave} = \frac{\overline{h}D_h}{k_{eff}} \tag{25}$$

In Eq. (25), D_h is the hydraulic diameter of the conduit whose value is given by Eq. (26).

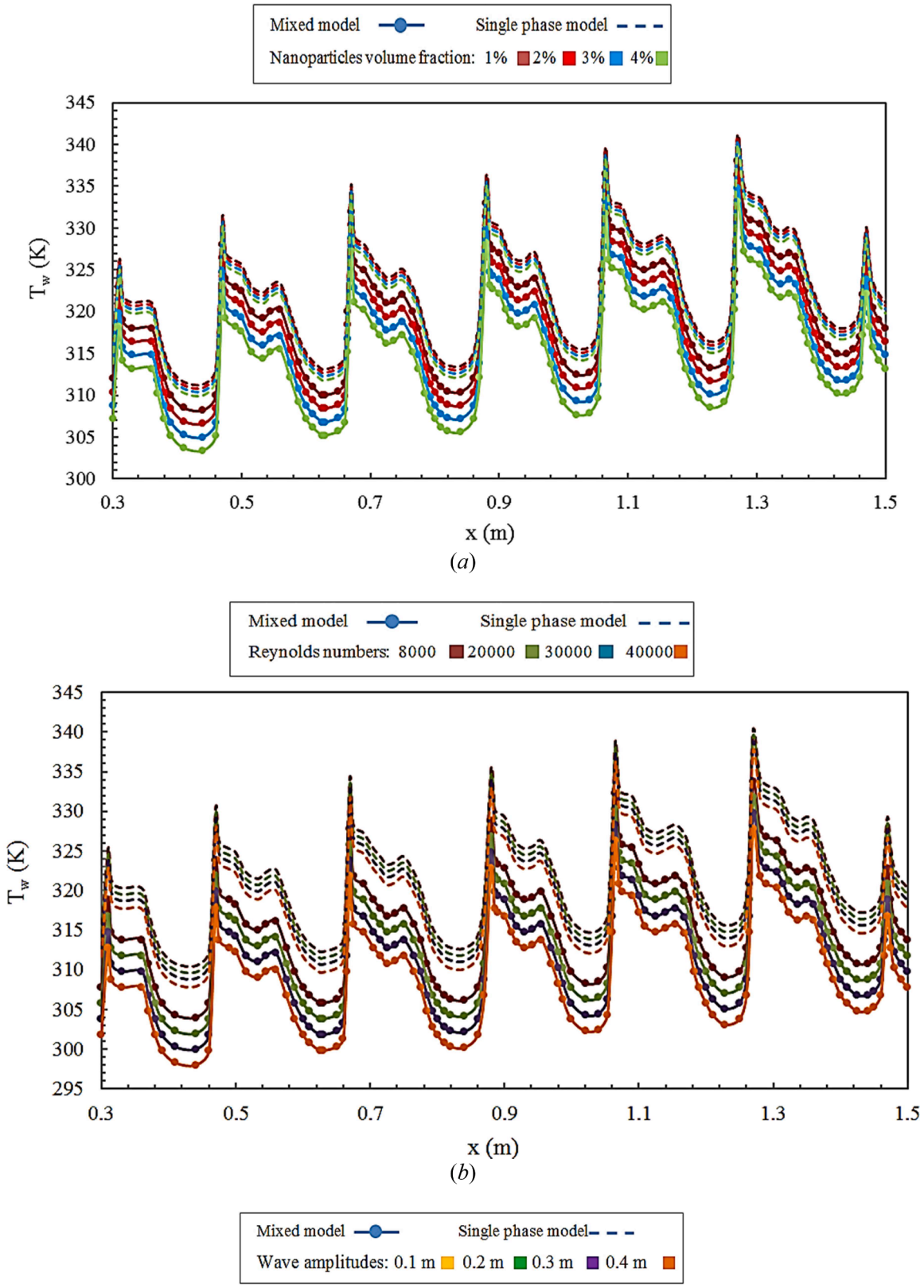

Fig. 5. The variation of wall temperature along the channel at different *a*) *SVFs* and $a = 0.3$ m & *Re*=8000, *b*) *Re* numbers and $a = 0.3$ m & *SVF* =3 % and *c*) wall amplitudes numbers and *Re*=8000 & *SVF* =3 % obtained by single phase and mixture models.

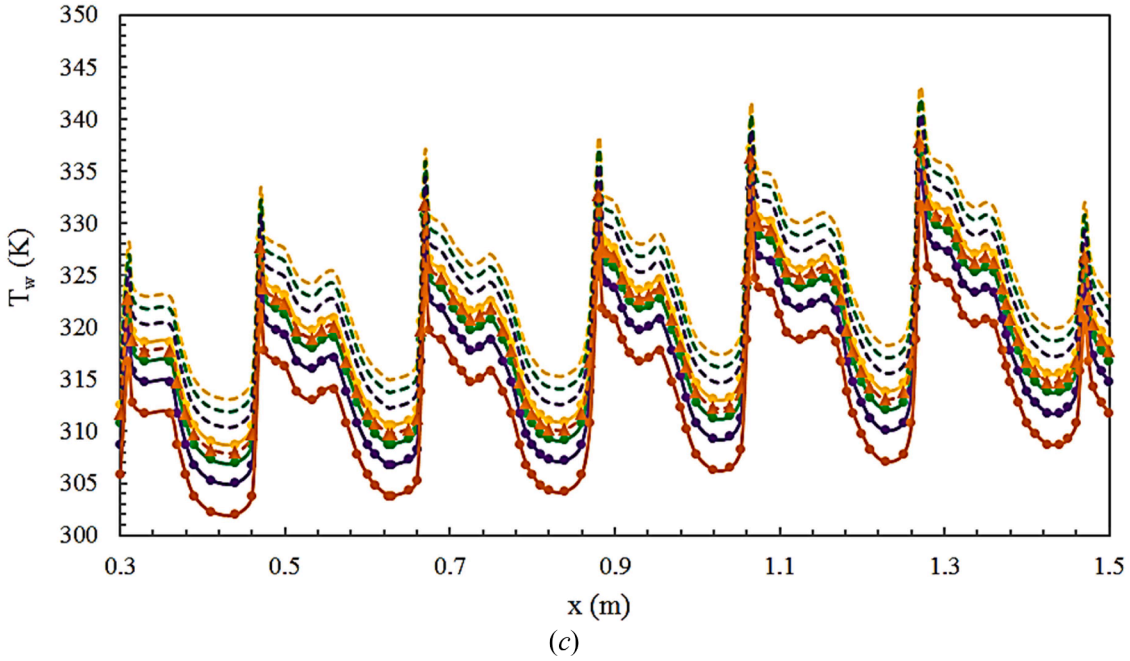

Fig. 5. (*continued*).

$$D_h = 4\frac{A}{P} = \frac{2wh}{(w+h)} \cong 2h \tag{26}$$

The presence of *NP*s affects both the heat transfer and fluid flow performance which could be described by heat transfer efficiency, or more accurately Colburn factor, and friction factor as denoted by Eqs. (27) and (28), respectively [41].

$$J = \frac{\mathrm{Nu}}{Re\ \mathrm{Pr}^{\frac{1}{3}}} \tag{27}$$

$$f = \frac{\tau}{\rho_m \frac{u_{in}^2}{2}} \tag{28}$$

3. Numerical method and validation

The governing equations alongside the corresponding boundary conditions are solved using the finite volume approach. The convective and diffusive terms of the governing equations are discretized using the second-order upwind and second-order central schemes, respectively. Considering the incompressible assumption made for modeling the *NF* flow, the *SIMPLE* algorithm is used for the pressure-velocity coupling. The structure is the *2D* squared structured type which for getting higher accuracy has been refined in high gradient areas near the walls. To ensure the independency of the obtained result from the employed mesh, the grid study is performed. Fig. 2 illustrates Nu_{avg} for different grid densities in *SVF* = 1 %. In addition, the numerical values of the Nu_{avg} for different grid sizes are shown in Table 3. It can be concluded that the grid with 550 × 100 cells is sufficiently fine to get independent results from the generated grid. A view of the applied mesh is shown in Fig. 3. The meshing process was done in Gambit and the solving procedure was conducted using Ansys Fluent.

To confirm the validity of the numerical method, Nu_{ave} for fully developed turbulent flow of *CuO*-water *NF* in the corrugated channel is compared against the results of Vanaki et al. [23] and Manavi et al. [44] (Fig. 4). Manavi et al. [44] investigated the thermal and flow performance of Al_2O_3 *NF* inside a wavy channel in a wide range of *Re* numbers using the two-phase model. Moreover, Vanaki et al. [23] studied the thermo-flow behavior of different *NF*s inside the channels with sinusoidal walls and with different *Re* numbers of 5000 – 18,000 and constant wall temperature. The figure shows a good agreement between the results of the present numerical model with that of the previous experimental data with a maximum deviation of 7 %. From the above comparisons, it is concluded that the employed *CFD* code is reliable and could be used to investigate the hydrodynamics and thermal behavior of the turbulent flow of the *NF*.

4. Results and discussion

By using the validated numerical code, the fluid flow and heat transfer are simulated in the channel. The system characteristics were evaluated using the wall and bulk flow temperatures, velocity profile, average and local *Nu* number in different *Re* numbers, *SVF*s, and wall amplitude numbers.

4.1. The variation of system indexes vs. the channel length

The wall temperature distribution along the channel axis versus the *SVF, Re* number and wavelength calculated by the mixture and single-phase modeling approaches and are shown in Fig. 5(a), (b) and (c), respectively. As shown, by increasing the *SVF* and due to the increased thermal conductivity of *NF*, the rate of heat transfer from the wall increased and the wall temperature decreased. In the mixture model, the wall temperature difference between different *SVF*s is more distinguishable than that in the single-phase model; in addition, the higher the *SVF*, the lower the wall temperature would be. Compared to single-phase modeling, the mixture model predicts a higher thermal conductivity for the fluid which results in a lower wall temperature. Another point that could be inferred from Fig. 5 is the overall increment of the wall temperature through the flow path which is the result of constant heat flux to the channel wall and despite the heat removal, would be augmented inside the wall. This increasing trend also follows the geometry of the channel; in the areas near the top of the wave and due to velocity increment, the wall temperature decreased and vice versa, near the concave areas, increased. Between the study cases, the lowest wall temperature is for the highest *SVF*, highest *Re* numbers and highest wave amplitudes which are due to the highest *Nu* numbers in these cases (Fig. 5).

Fig. 6 shows the bulk fluid temperature along the channel axis versus

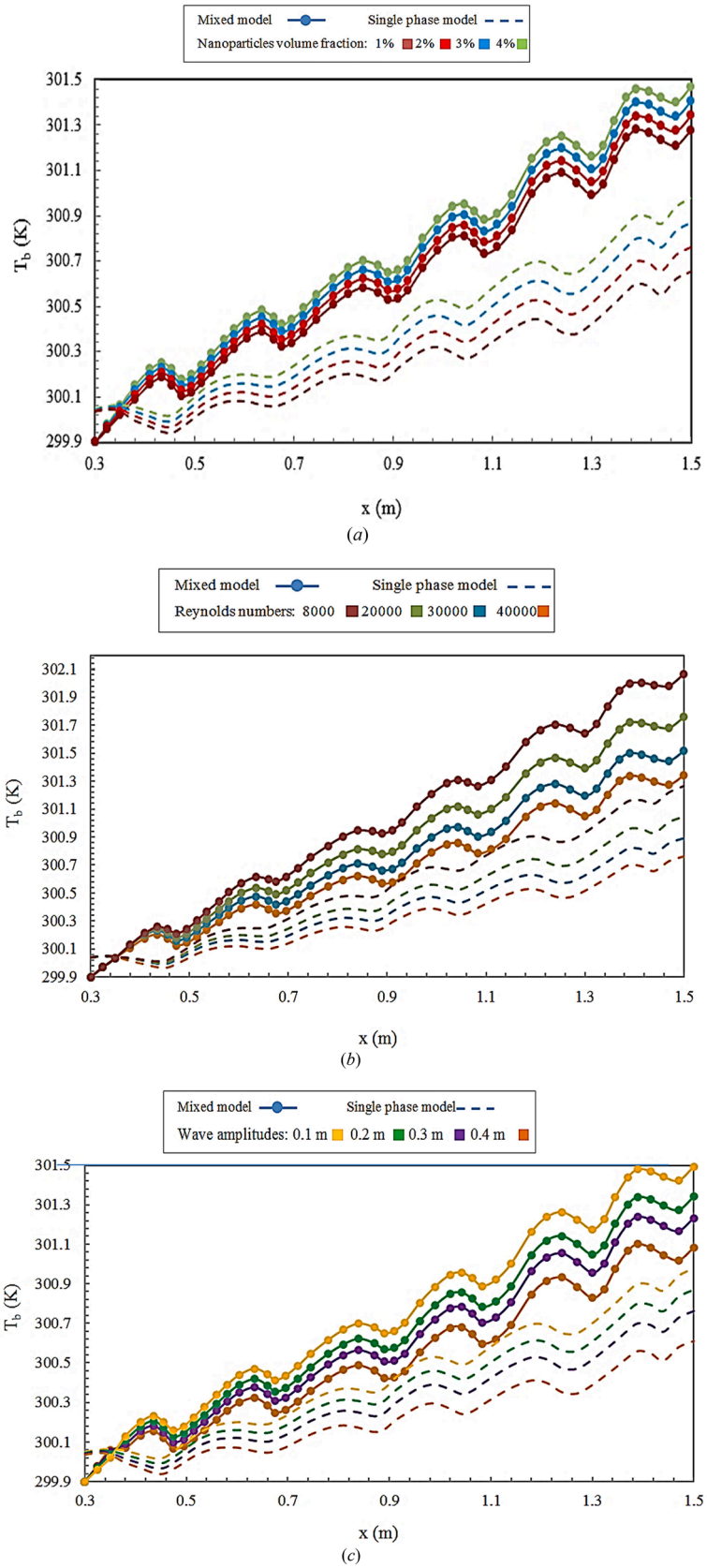

Fig. 6. The variation of bulk fluid temperature along the channel length at different *a*) *SVFs* and $a = 0.3$ m & *Re*=8000, *b*) *Re* numbers and $a = 0.3$ m & *SVF*=3 % and *c*) wall amplitude numbers and *Re*=8000 & *SVF*=3 % obtained by the mixture and single-phase modeling.

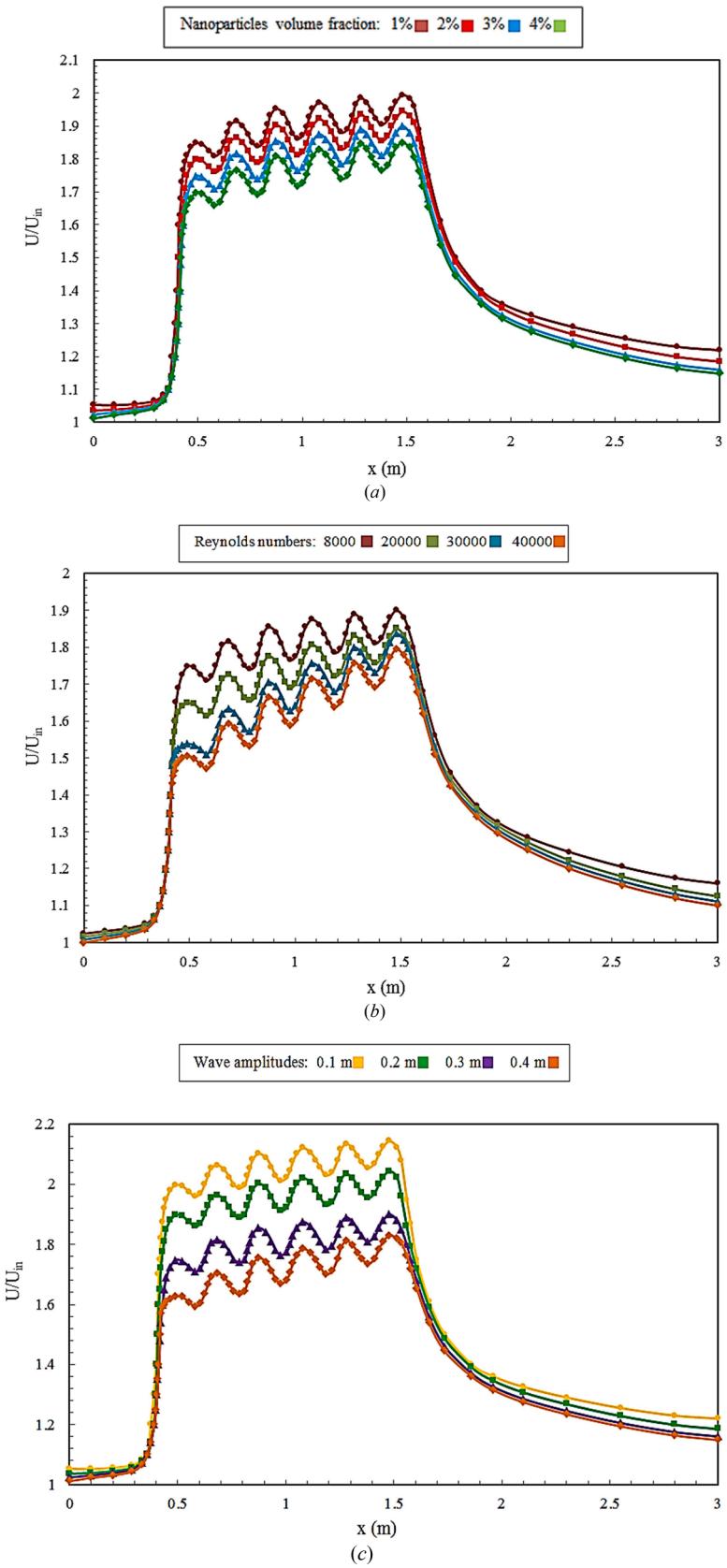

Fig. 7. The variation of dimensionless axial velocity along the channel centerline in different *a*) *SVFs* and $a = 0.3$ m & *Re*=8000, *b*) *Re* numbers and $a = 0.3$ m & *SVF* =3 % and *c*) Wall amplitude numbers and *Re*=8000 & *SVF* =3 %.

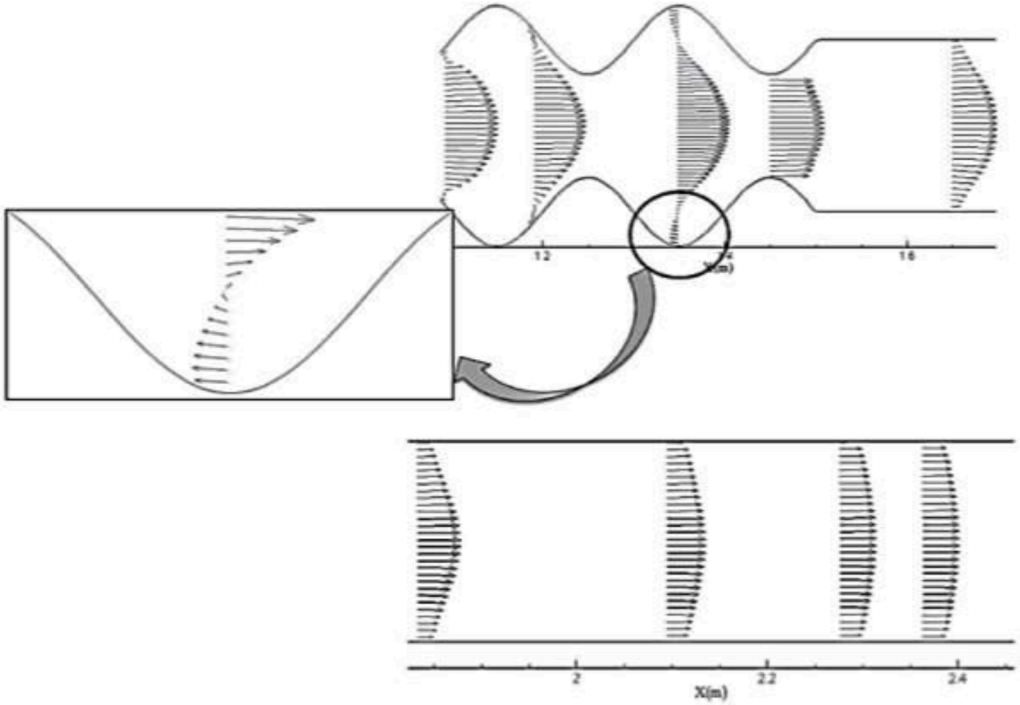

Fig. 8. Velocity profile in different channel sections at *Re*=20,000, *SVF*=0.03 and $a = 0.3$ m.

the parameters of *SVF* (a), *Re* number (*b*), and wavelength (c). As could be seen, like the wall temperature the overall bulk fluid temperature along the channel length is increasing. Comparing the bulk fluid temperature obtained by the mixture and single-phase models, the former model shows the higher temperature; also, by increasing the *SVF* in both models and due to the increased thermal conductivity of *NF*, the fluid temperature would be increased. It could also be observed that the temperature difference between different study cases increased through the channel length; at $x = 1.5$, the bulk temperature difference is 0.2, 0.76 and 0.44 between *SVF* of 0 and 4 %, *Re* of 8000 and 40,000 and wave amplitudes of 0.1 and 0.4, respectively, where the corresponding values are zero at the entrance ($x = 0$). This shows that the heat transfer improving effect of increasing *Re* number, *SVF,* and wave amplitude becomes more significant by distancing from the entrance region; in other words by departing from the entrance region, the effect of heat transfer improving factors augments which increases the bulk fluid temperature more. In addition, in the flow path, the difference between the results of the mixture and single-phase models increased and the bulk temperature in the mixture model is approximately 5 % higher than in the single-phase model; this shows that by increasing flow time, the accuracy of the single-phase model decreased.

Fig. 7 shows the centerline axial velocity distribution in dimensionless form along the channel length versus the *SVF* (*a*), *Re* number (*b*), and wavelength (*c*). By inspecting the figure, an increasing trend could be observed vs the *SVF*s, *Re* numbers, and wave amplitudes increment. The overall increment of centerline velocity through the flow path which is the result of the formation and growth of the vortices in the flow path has an intermittent nature; these fluctuations are the result of the formation of vortices in the recesses of the waves and the formation of backflow. As could be seen in Fig. 7(a), increasing the *SVF*, decreases the centerline velocity, particularly in wavy regions of the channel; by increasing the *SVF* from 1 % – 4 % the dimensionless velocity decreased by 0.16 in the corrugated area and remains nearly unchanged in the smooth zone. The higher effect of *NP* increment on decreasing the axial velocity in the corrugated zone comes back to the existence of vortices and therefore, the higher effect of fluid viscosity on velocity reduction. As shown in Fig. 7(b), after $x = 2.8$ and for all *Re* numbers a fully developed region could be observed, which is the result of continuous flow in the smooth channel. By the *Re* number increment, the beginning of the flow development moves downstream because the increased axial velocity transmits the generated perturbation in the flow direction, the center line velocity is also reduced, which is the result of a more uniform velocity profile at higher *Re* numbers.

For better visualizing the hydrodynamics of fluid, the velocity profile in different channel sections at *Re*=20,000, *SVF*=0.03 and $a = 0.3$ m is depicted in Fig 8. As seen, the fluid has its maximum velocity in the converging section through the channel way. In each section, the maximum velocity is in the centerline and the minimum is in the vicinity of walls; a collision of fluid particles to wall dissipates its energy and the reverse flow is created. In the center of the depression zone, the velocity becomes nearly zero and negative toward the wall. The reverse and main flow collision generates vortexes near the wall. By adding *NP*s and increasing their concentration in *NF*, the fluid velocity increases in both forward and backward directions which increase the vortex strength which enhances the wall-fluid heat transfer. At the end part, by eliminating the wavy shape, the vortex generation stopped and the flow get gradually developed and a nearly uniform profile is generated.

Fig. 9 shows the variation of Nu_{avg} versus the phase lag in different *SVF* (*a*), *Re* number (*b*), and amplitude values (*c*). The increment of the Nu_{avg} for angles of less than 180 ° is due to the shrinkage of vortices where an improvement of 7.5 % was observed. Changing the phase difference of the wave changes the behavior of the flow in such a way that the vortices will not have enough time to grow. These vortices trap some of the fluid inside, preventing the cold fluid from coming into contact with the hot wall. Therefore, their shrinkage increases the temperature gradient and, consequently, increases the *Nu* number and heat transfer. It could also be seen that, between the study cases the highest *Nu* number is for the highest *SVF* (*SVF*=4 %), *Re* number (*Re*=80,000), and wall amplitude ($a = 0.4$ m).

The distribution of the *Nu* number along the channel length in different *SVF, Re* numbers, and wavelengths, is depicted in Fig. 10(a), (b), and (c), respectively. As could be seen, for different study cases, the overall variation of local *Nu* number vs. the channel length is decreasing with a small declination rate. This downward trend is due to get heating

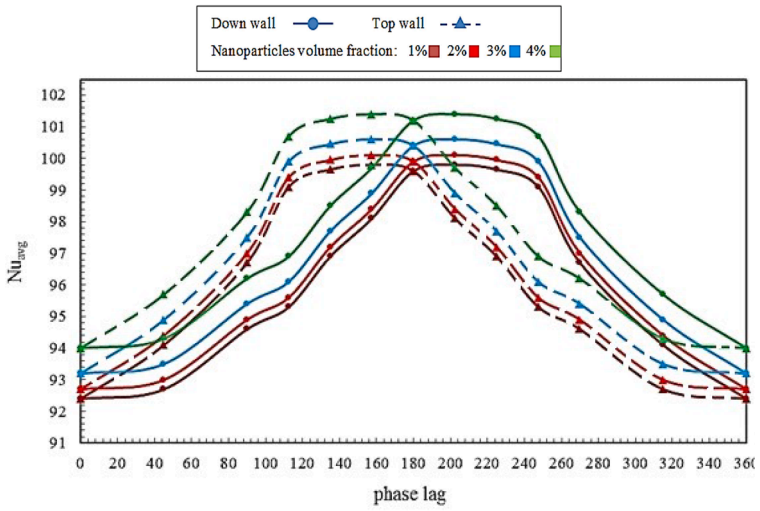

(*a*)

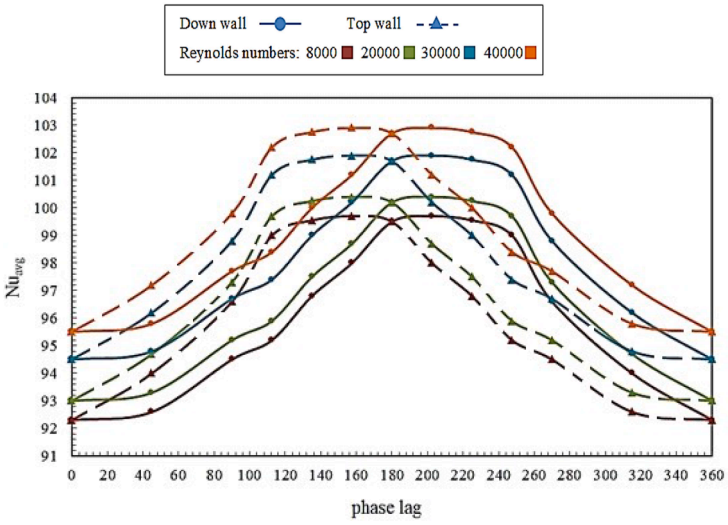

(*b*)

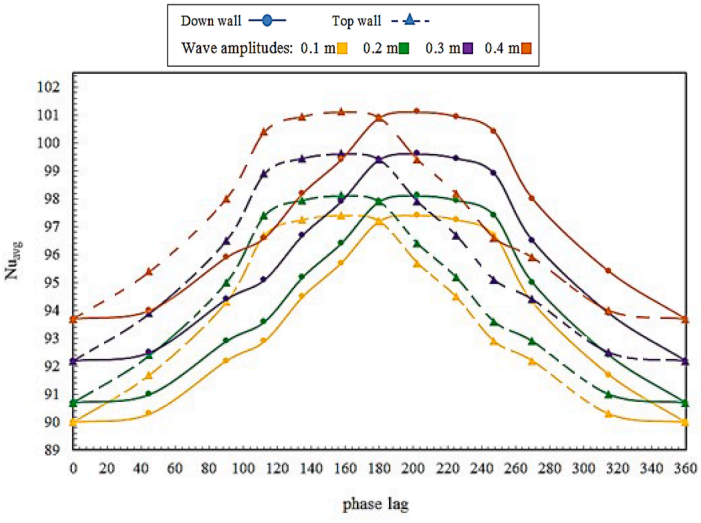

(*c*)

Fig. 9. The variation Nu_{ave} vs the phase lag in different *a*) *SVFs* and $a = 0.3$ m & *Re*=8000, *b*) *Re* numbers and $a = 0.3$ m & *SVF* =3 % and *c*) Wall amplitude numbers and *Re*=8000 & *SVF* =3 %.

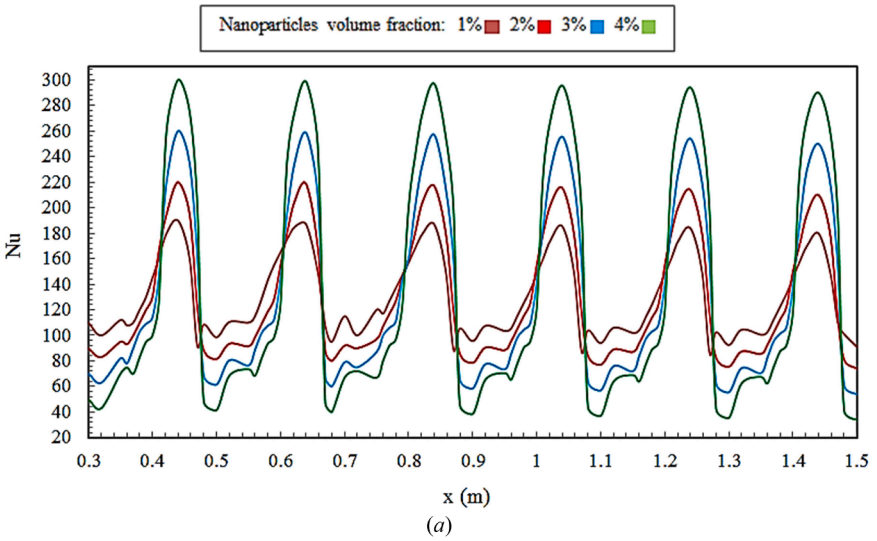

(*a*)

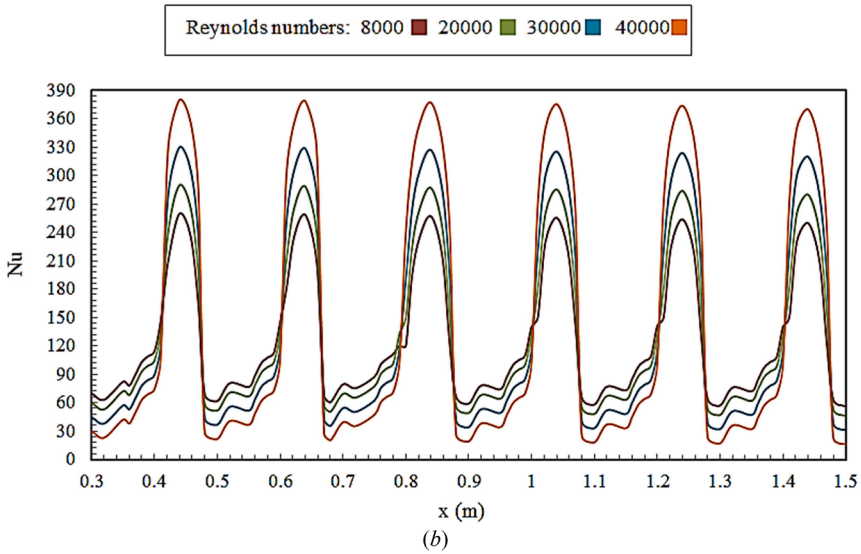

(*b*)

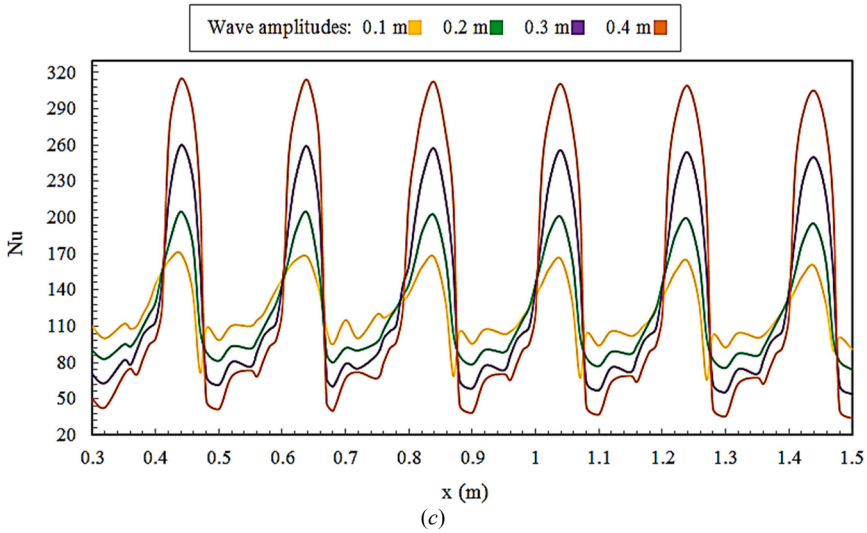

(*c*)

Fig. 10. The variation *Nu* number vs the channel length in different *a*) *SVFs* and $a = 0.3$ m & *Re*=8000, *b*) *Re* numbers and $a = 0.3$ m & *SVF* =3 % and *c*) Wall amplitude numbers and *Re*=8000 & *SVF* =3 %.

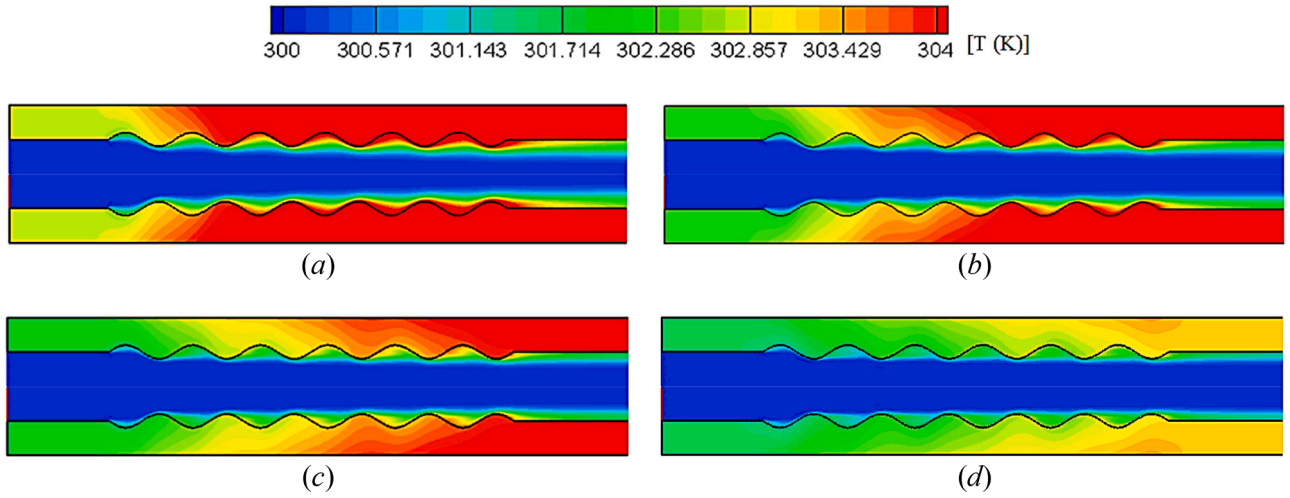

Fig. 11. Temperature contours of the wall and fluid flow in different Re numbers of *a*) 8000, *b*) 20,000, *c*) 30,000 and *d*) 40,000.

of the fluid and the temperature gradient decrement along the channel length. Another point that can be seen in the figure is the waveform variation of the local *Nu* number along the channel; at the ridges of the wall and due to the velocity increment, the local *Nu* number is the highest, behind it the *Nu* number decreased due to flow separation. In the zero amplitude section, a decreasing trend could be seen. At higher wavelengths, the local *Nu* number in indentations has a sharp decline in such a way that it becomes less than Nu_{avg}. This phenomenon which is due to the formation of vortices is in contrast to the situation in the protrusions. In protrusions the *Nu* number has a sharp increment due to the highest temperature gradient there which, increases Nu_{avg}; for wall amplitude number of $a = 0.3$ m, *SVF*=0.03 and the *Re*=8000, the Nu_{avg} is 2.3 times than that in the smooth wall.

4.2. The influence of Re number

The temperature contour of fluid flow for *SVF*=3 % in different *Re* numbers is shown in Fig. 11. As can be seen, by exerting the heat flux to the channel wall, the fluid temperature increased along the channel length and, with increasing the *Re* number, and due to continuous and periodic reconstructions of the thermal boundary layer, the rate of heat transfer increased rapidly. By increasing the *Re* number and the resulting flow velocity and turbulence, the penetration of cold fluid into the channel wall increases and reduces the wall temperature, and as shown in Fig. 11, from the *Re*= 8000 – 40,000, the internal wall temperature at the end of the channel dropped from 304 K to approximately 303 K. The *Re* number increment which is associated with velocity increase has a positive effect on cooling the wall; moreover, decreases the stationary zones inside the wall depression and prevents the possibility of the formation of hot spots in these regions. The temperature reduction of the channel wall by the *Re* number increase confirms the growth of the heat transfer rate.

To justify the temperature contour inside the channel, the flow streamlines at different *Re* numbers are depicted in Fig. 12. As seen, the vortex flows are weak at initial lengths and become more and stronger along the way. Also, all cavities are filled with vortexes and by the *Re* number increment, the vortex number and their intensity increase too, which improves the heat transfer rate.

The variation of Nu_{avg} vs the *Re* number at *Re* numbers of 8000, 20,000, 30,000, and 40,000 and *SVF*=0.01, 0.02, 0.03, and 0.04 and different wavelengths shown in Fig. 13. As the *Re* number increased, the Nu_{avg} shows an upward trend. As shown in Fig. 13, the mixture model outputs a higher Nu_{avg} than the single-phase model; for example at *Re*= 40,000 and *SVF*=0.03 and wavelengthα =0.3 m, Nu_{avg} is approximately 1.1 times of the single-phase model. This approves the higher accuracy of the mixture model to predict the performance of *NF* flow. By inspecting Fig. 13 it is revealed that the Nu_{avg} increased by increasing the *SVF, Re* number and wall amplitude increment. The improvement of Nu_{avg} resulting from the *SVF* increment is mainly due to the increase of the effective thermal conductivity of the *NF* compared to the base fluid; this would reduce the temperature difference between wall and fluid which eventually increases the heat transfer coefficient and *Nu* number under constant heat flux input. As the *Re* number increased, the axial velocity increased and the heat penetration from the channel wall into the central region of the fluid flow increased, resulting in the growth of the heat transfer rate. It is worth noting that *SVF* increment does not work the same in different *Re* numbers and has a higher improving effect in lower *Re* numbers; in the case of wall amplitude of 0.1 m, by increasing the *NF* concentration from 1 – 4 % the Nu_{avg} increases by 35 % and 22 % in *Re*= 8000 and 40,000, respectively. This behavior, which is also observed in other wall amplitudes, suggests the higher effect of using *NF* where the other enhancing factors are absent. A similar situation exists in the case of wave amplitude increment; the Nu_{avg} improvement resulted from increasing the *SVF* from 1 % – 4 % ceases by increasing the wave amplitude value and is 35 %, 25 %, 18 %, and 14 % for amplitudes of 0.1, 0.2, 0.3 and 0.4 m, respectively. This shows that the enhancing effect of using *NF* is more significant where the effect of other enhancing factors (such as the *Re* number or *SVF* increment) is weak.

4.3. The effect of wave amplitude number

To reveal the effect of wave amplitude number, the temperature contour of the channel wall (thickness of 0.1 m) and fluid flow for different wall amplitudes are illustrated in Fig. 14. As can be seen, increasing the wall amplitude disrupts the behavior of the fluid and increases the penetration of heat into the fluid flow. The heat penetration by the wave amplitude increase could be seen in thinning the cold center line. As the amplitude of the wave increased, the separation rate behind the sinusoidal convex portion became more intense (Fig 8) which had a significant effect on the flow. At higher amplitudes, the velocity at the top of the wave increases which enhances the pressure gradient behind the wave. Increasing the velocity along with increasing the turbulence and mixing of the flow will increase the heat transfer rate. The increased heat transfer rate has also a positive effect on cooling the wall and could postpone its overheating to later. To reveal the effect of wave amplitude on temperature contour, the flow streamlines at different amplitude numbers and *Re*=20,000 is shown in Fig. 15.

As seen in Fig. 15, by increasing the wave amplitude, the separation region behind the convex region becomes larger. At the smallest

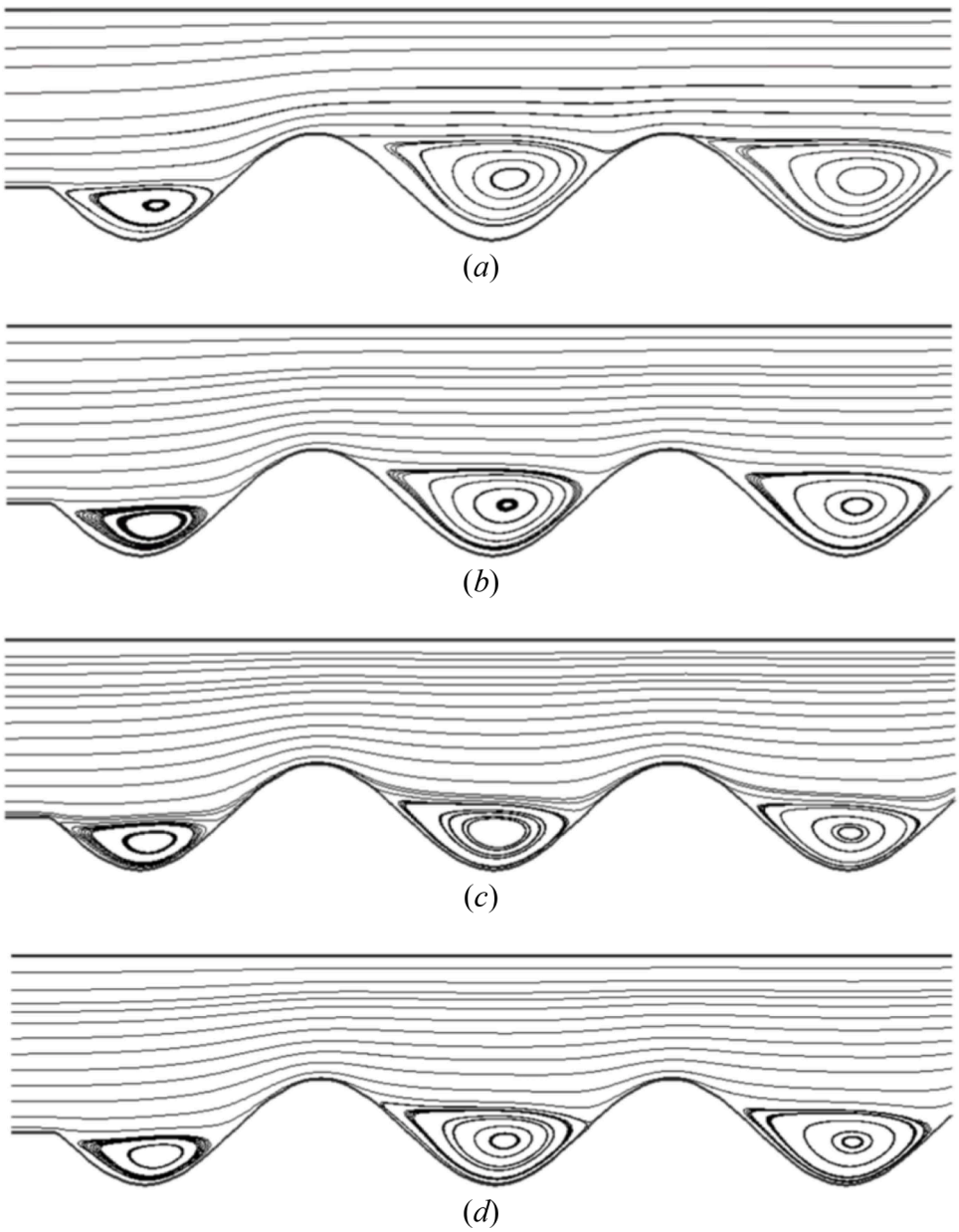

Fig. 12. Flow streamlines at different *Re* numbers of *a*) 8000, *b*) 20,000, *c*) 30,000 and *d*) 40,000 for $a = 0.3$ m and *SVF*=0.03.

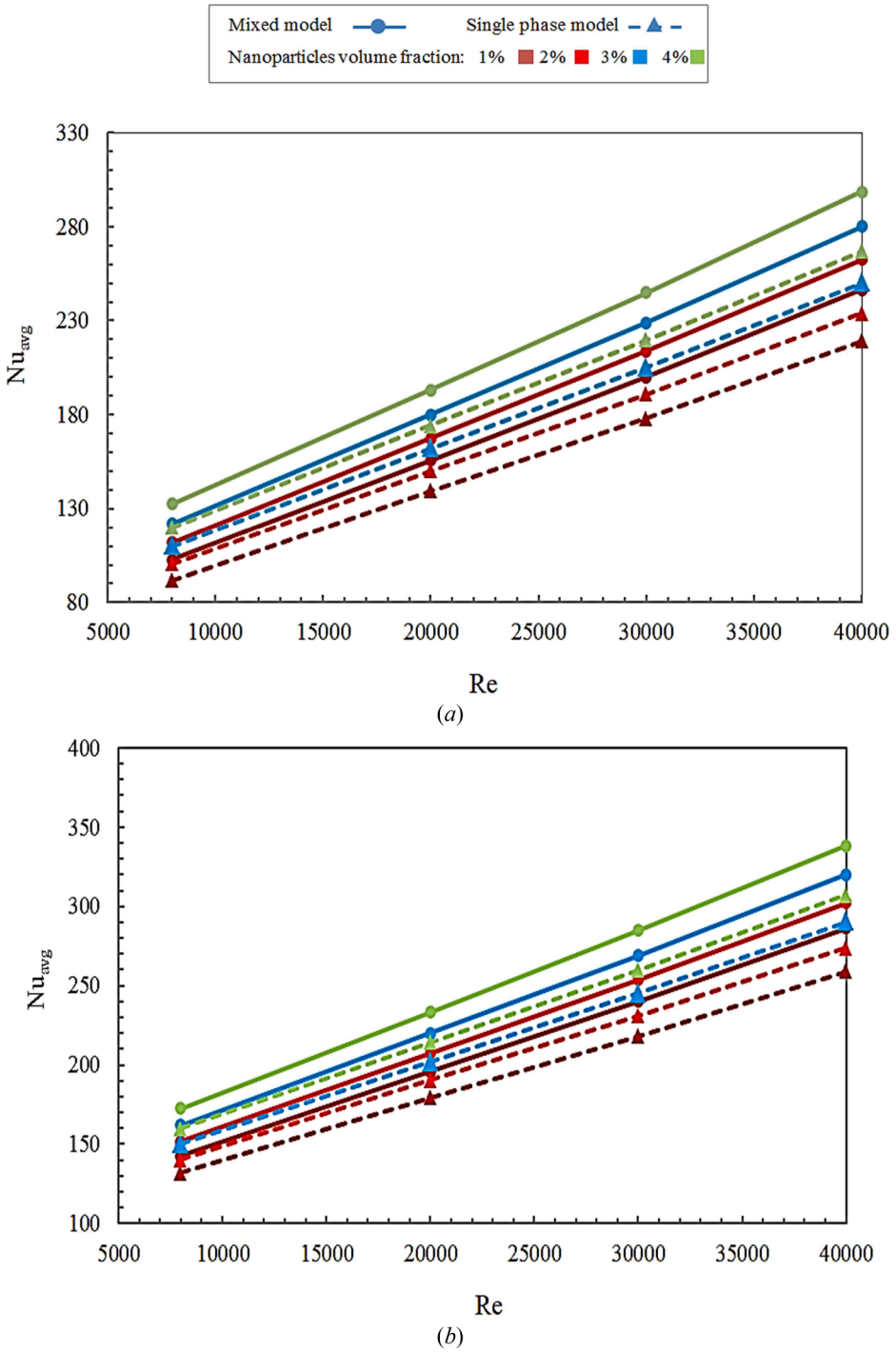

Fig. 13. Comparison of the *Nu* number in single-phase and mixture models at different wavelengths of *a*) 0.1 m, *b*) 0.2 m, *c*) 0.3 m and *d*) 0.4 m.

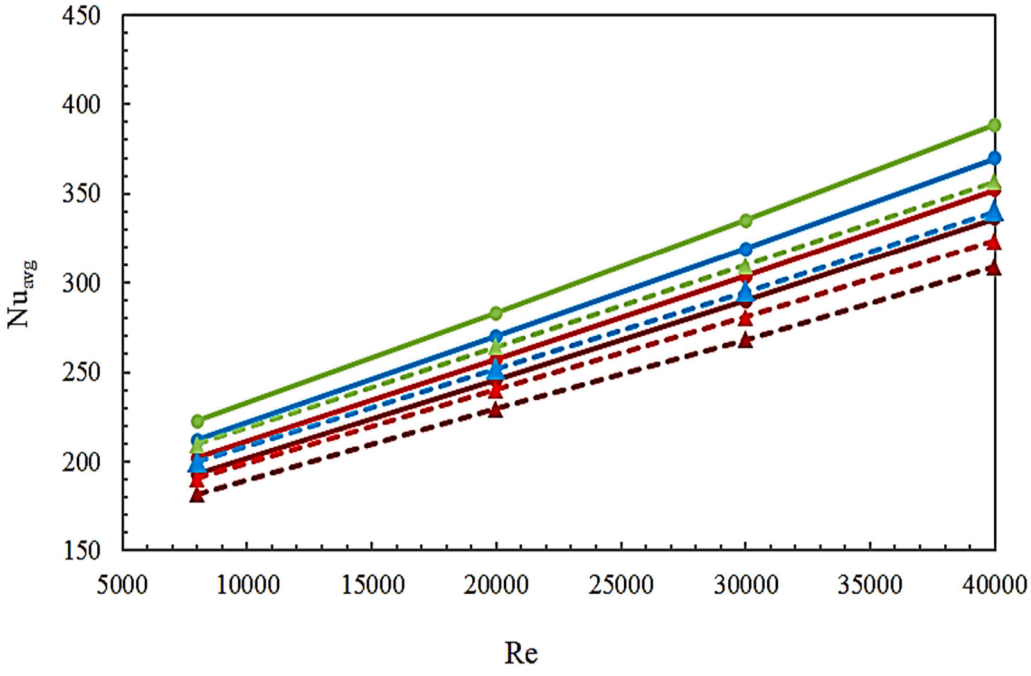

(*c*)

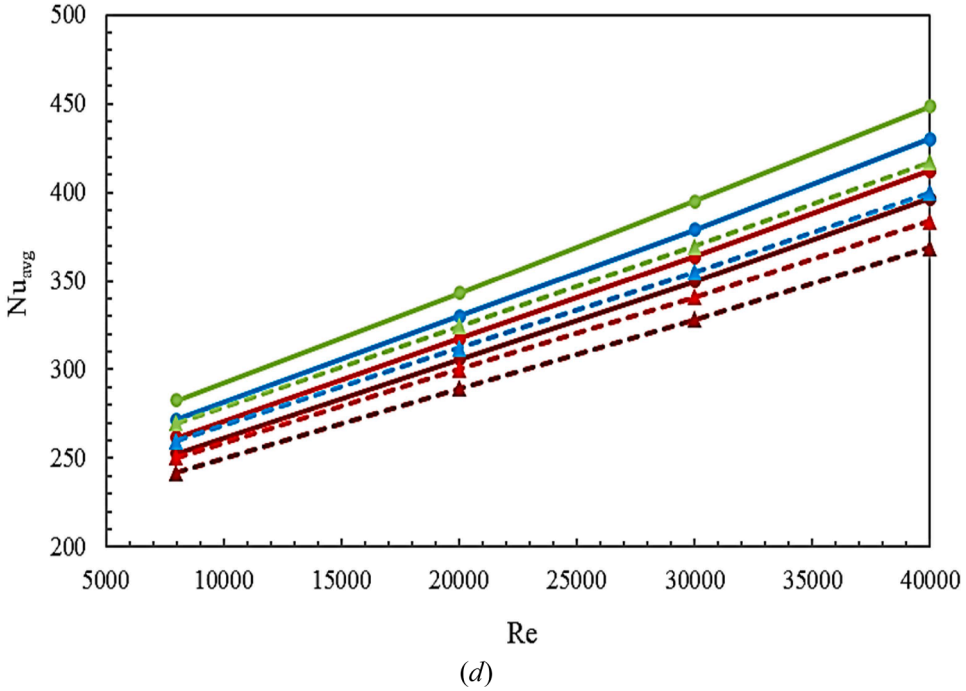

(*d*)

Fig. 13. (*continued*).

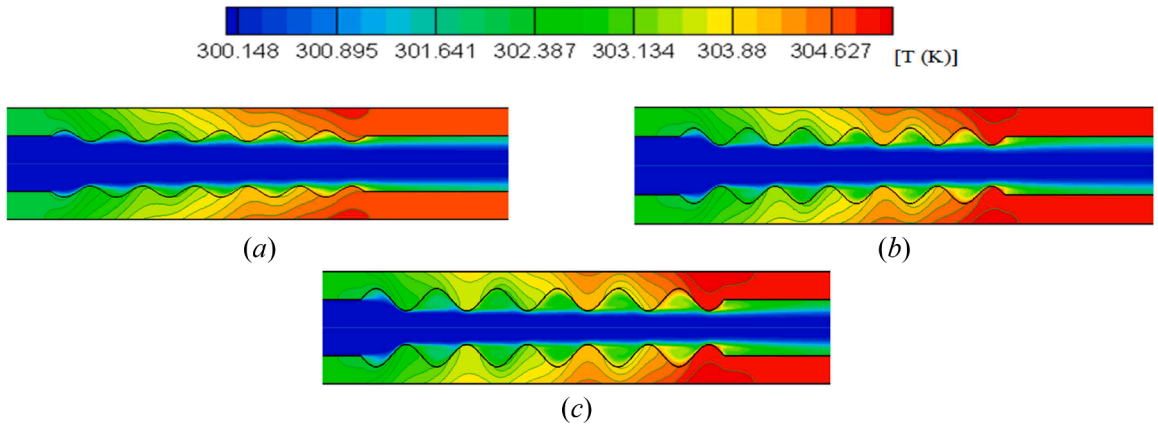

Fig. 14. Temperature contour for wave amplitudes of *a*) 0.2, *b*) 0.3 and c) 0.4 m and *Re*= 20,000.

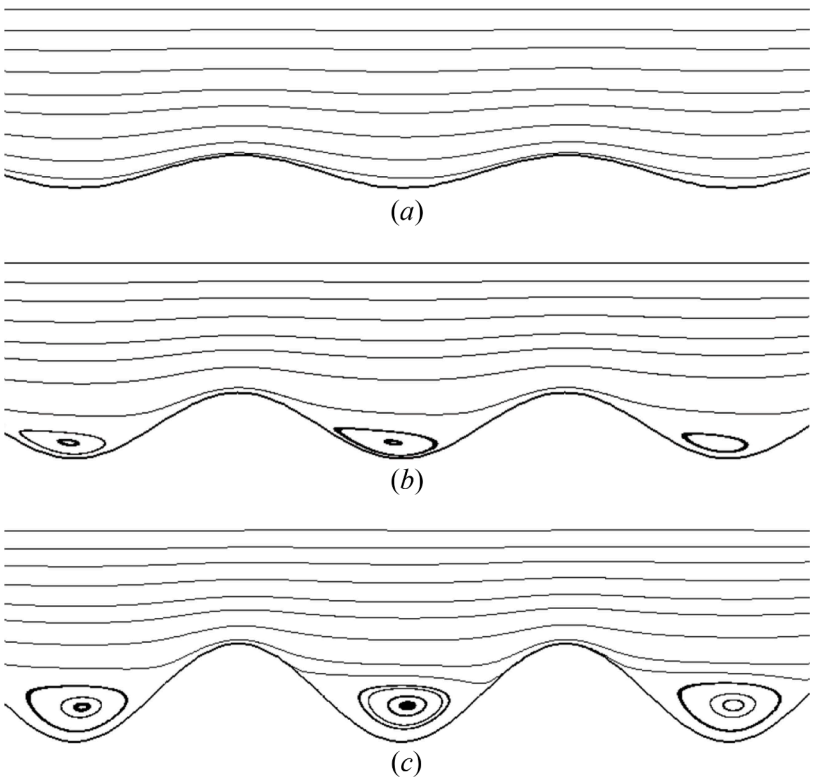

Fig. 15. Flow streamlines for different amplitude values of *a*) 0.1 m, *b*) 0.2 m and *c*) 0.3 m for *Re*=20,000 and *SVF*=0.03.

amplitude value, i.e. $a = 0.1$ m, the reverse flow has not been observed and by the wave amplitude increase, put forward the separation point toward the dome; this would increase the separated region length and consequently increase the heat transfer coefficient and friction factor.

The variation of the Nu_{avg} versus the wave amplitude for different values of *Re* numbers and *SVF* are shown in Fig. 16(*a*) and (*b*), respectively. As could be seen, the overall variation of Nu_{avg} vs the wave amplitude in different *Re* numbers and *SVFs* are increasing; in a specific *SVF* and *Re* number, and by the wave amplitude increment from 0 – 0.4 m, Nu_{avg} increases by nearly 50 %. By increasing the wave amplitude and by the emergence of rotational flows behind the wave and the reverse flow process, the Nu_{avg} decreased; on the other hand, Nu_{avg} is grown by the increased velocity in the convergence part of the channel. As the flow passes through the curves of the channel, the symmetrical flow and turbulence form which eventually leads to excessive mixing of fluids and the increased heat transfer rate. Also, it could be seen that with the *Re* number increment, Nu_{avg} increases too; as the *Re* number increases from 8000 – 40,000, the Nu_{avg} increases approximately by 75 %.

As an important factor from the viewpoint of fluid flow, the pressure drop, versus the wavelength at different *SVF* and *Re* numbers are shown in Fig. 17(a) and (b), respectively. The pressure drop is determined by subtracting the average outlet pressure from the inlet one. As expected, the pressure drop increased with increasing wave amplitude, *SVF*, and *Re* number; from a wavelength of 0.1 m – 0.4 m, the pressure drop in the case of *Re*=8000 and *SVF*=1 % increased by 73 % (from 0.12 *Pa*– 0.45 *Pa*). The pressure drop in corrugated ducts is higher than in flat-walled ducts due to the collision of the fluid with the ridges of the duct wall and the subsequent formation of vortices. It could be also revealed from Fig. 17(a) and (b) that the pressure drop inclination rate vs. the amplitude number is the highest in cases of the highest *SVF* and *Re* number; by increasing the wave amplitude number from 0.1 – 0.4 the pressure drop increment is 2.67 and 2.7 times for *SVF* value of 1 % and 4 % and 1.6

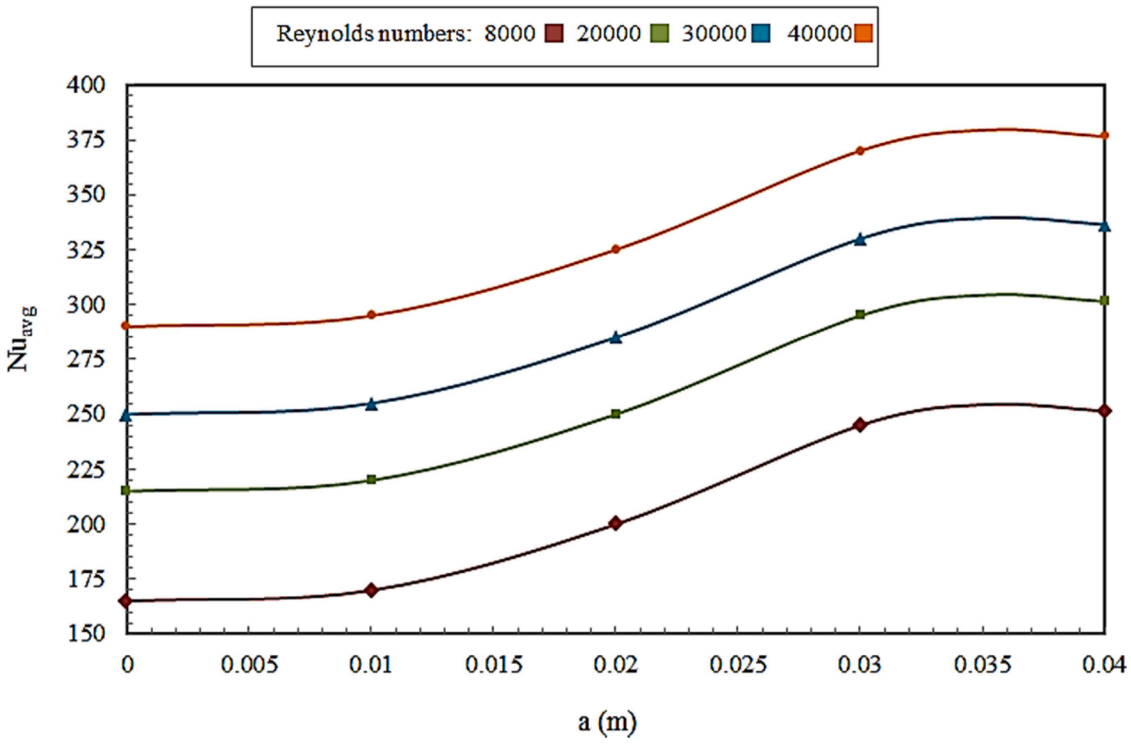

(*a*)

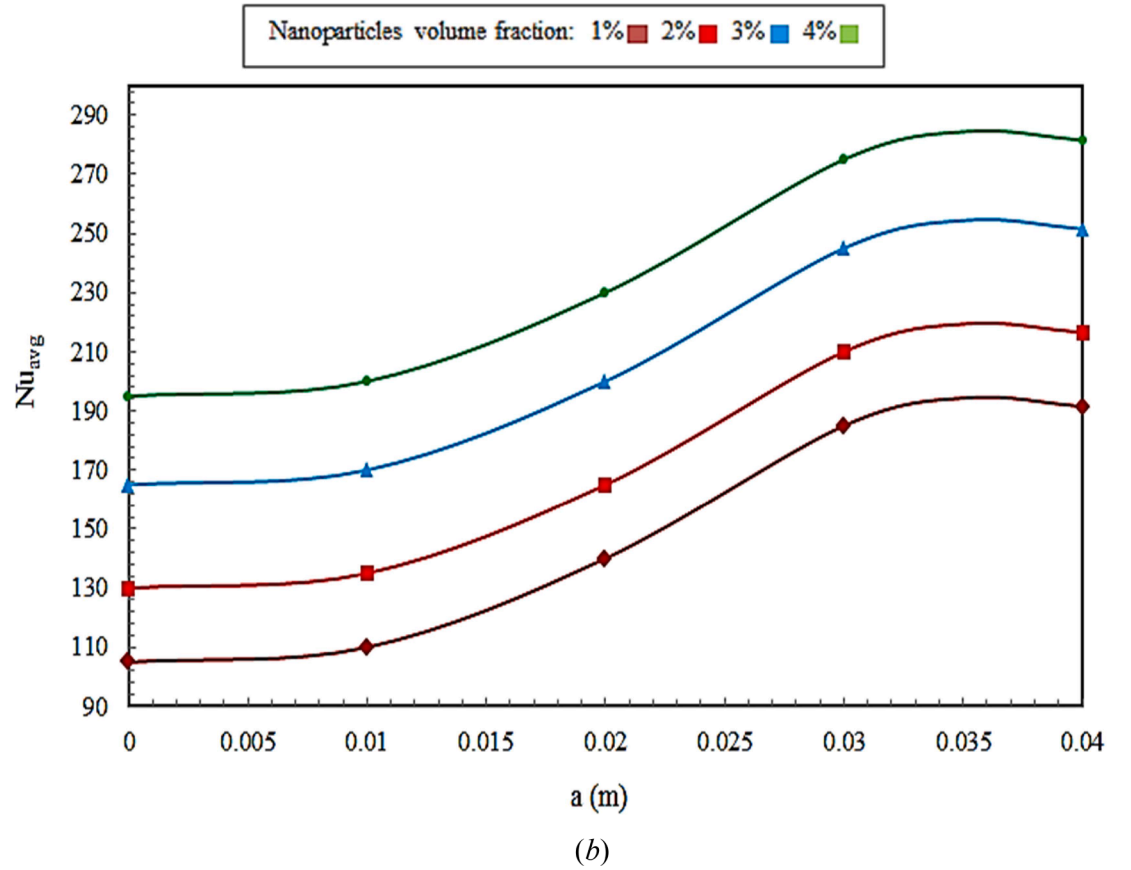

(*b*)

Fig. 16. The Nu_{ave} vs. the wave amplitude in different *a*) *Re* numbers and *SVF*=3 % and *b*) *SVFs* and *Re*=8000.

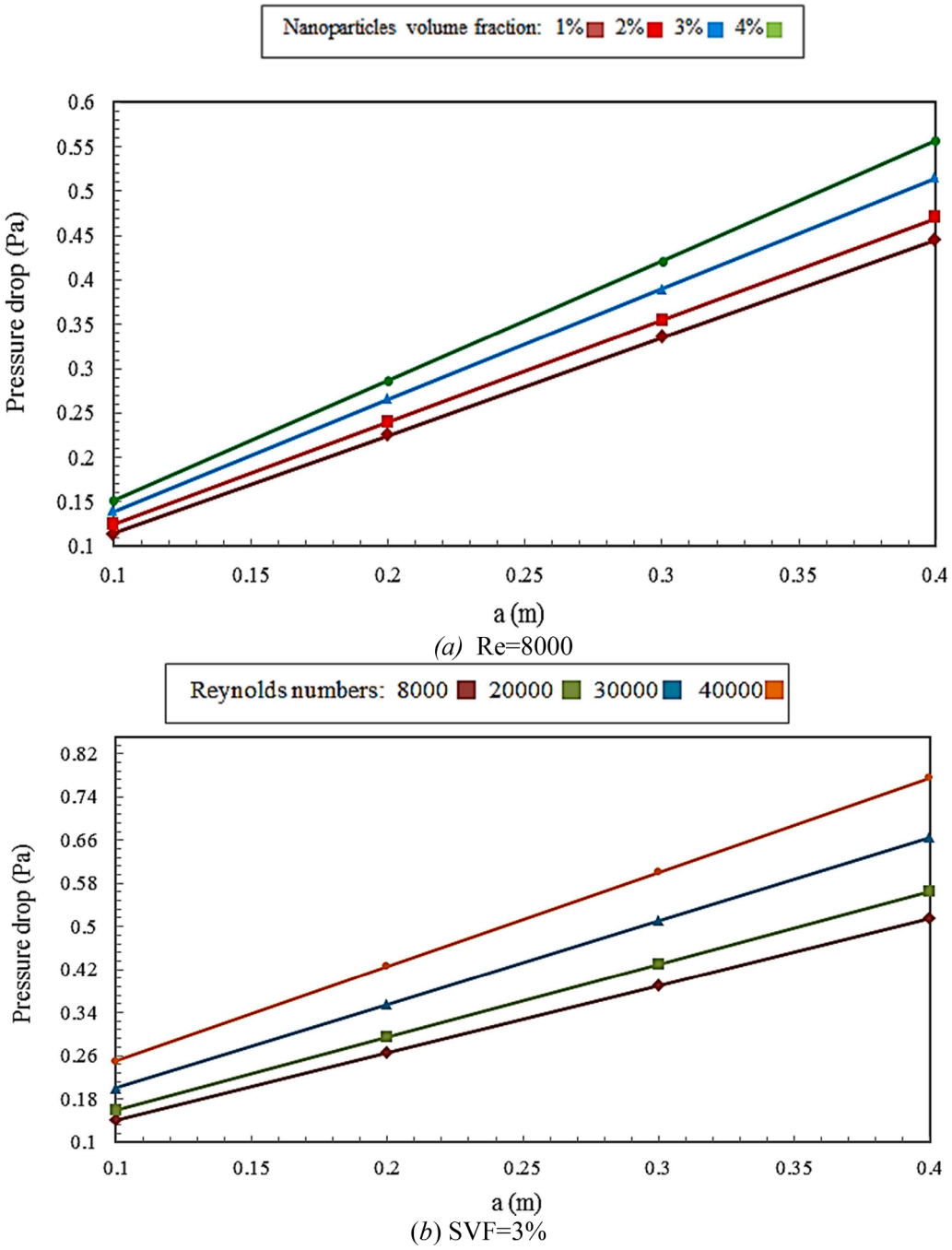

Fig. 17. The flow pressure drop vs the wave amplitude number in different *a*) *SVFs, b*) *Re* numbers.

times and 2.7 times for *Re*=8000 and 40,000, respectively. This demonstrates the more beneficial effect of increasing the *SVF* than increasing the *Re* numbers on system performance under the present operating conditions.

4.4. The effect of SVF

The addition of *NP*s to the fluid increases both the values of heat transfer and pressure drop; to reveal the effect of using *NP* on the overall thermo-flow characteristics of the system, the *J/f* factor is used, as the quotient Eq. (27). The variation of *J/f* factor vs. the *SVF* for different wave amplitudes and *Re* numbers are shown in Fig. 18(*a*) and (*b*), respectively. The figure shows the improving effect of increasing *SVF* on the value of *J/f* at each *Re* and wave amplitude numbers; at wave amplitude of $a = 0.3$ m and by increasing the *SVF* from the *SVF* =0.01 to *SVF*=0.04, the *J/f* increases by 30 %. This approves the heat transfer improving effect of *SVF* increment is greater than pressure drop increment at all *Re* numbers and wall amplitudes. Also, the *Re* number increment harms *J/f* value, and by being increased from 4000 – 80,000, *J/f* deteriorates by approximately 75 %.

5. Conclusion

Considering the widespread application of heat exchangers in industry, heat transfer improvement in these devices became an inevitable task. The *NF*s by their superior thermal properties are a good choice for this purpose. In this work, the application of *CuO*/water *NF* in a corrugated channel heat exchanger was studied. The heat exchanger surface is

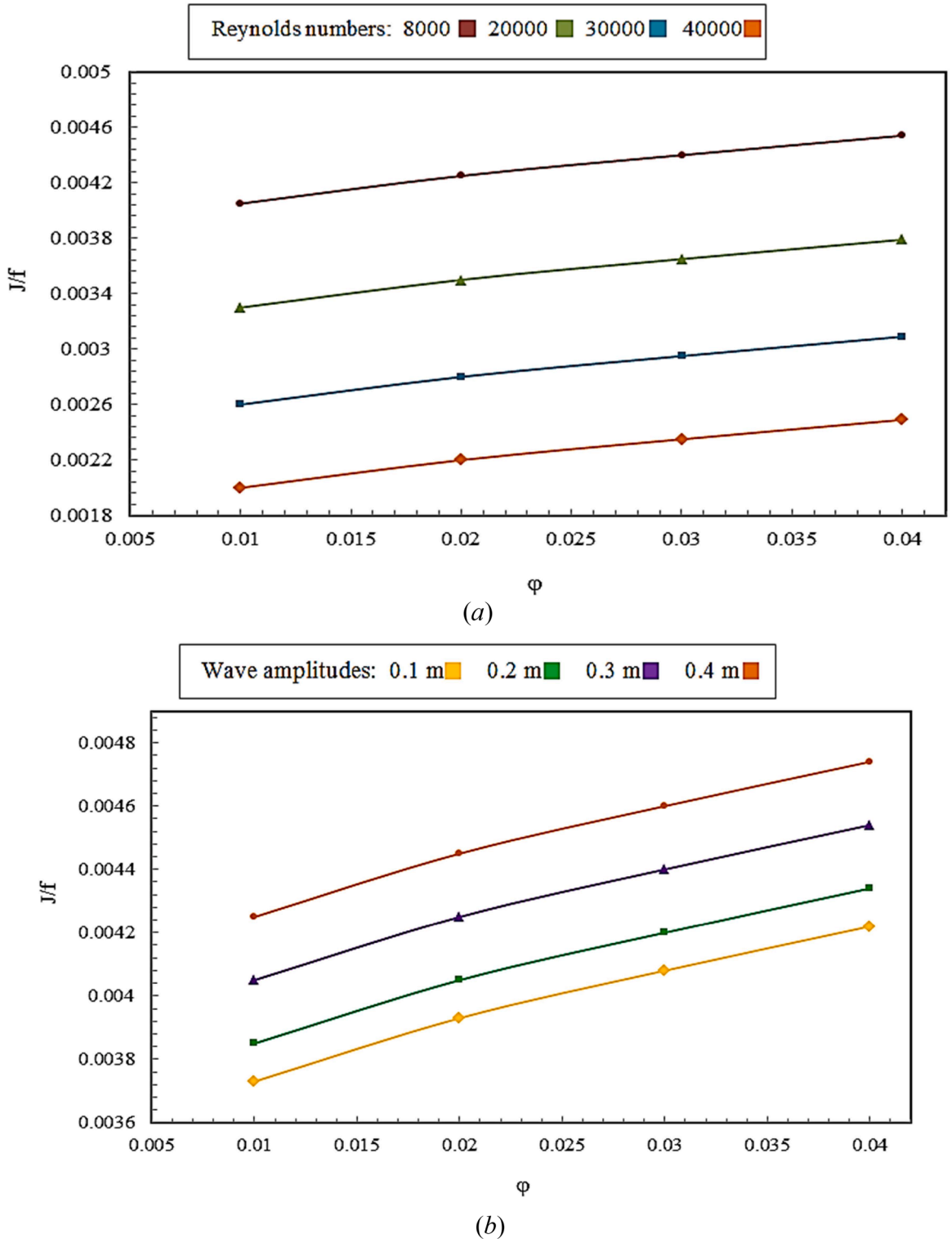

Fig. 18. The J/f factor vs the *SVF* in different a) *Re* numbers and $a = 0.3$ and b) wave amplitudes and *Re*=8000.

under a constant heat flux and the thermal and fluid flow performance of *NF* is simulated using the two-phase mixture model. The obtained results could be summarized as follows.

- Compared to single-phase modeling, the mixture model predicts a higher thermal conductivity for the fluid which results in an increased higher heat removal rate and lower wall temperature.
- Between the study cases, the lowest wall temperature is for the highest *SVF*, highest *Re* numbers and highest wave amplitudes which is due to the highest *Nu* numbers in these cases and the result of more intensified turbulent flow.
- The temperature difference between different study cases increased through the channel length. This shows that the heat transfer enhancing effect of increasing *Re* number, *SVF*, and wave amplitude becomes more prominent by distancing from the entrance region; in

other words by departing from the entrance region, the effect of heat transfer improving factors augments which increases the bulk fluid temperature more.

- Increasing the *SVF*, decreases the centerline velocity, particularly in wavy regions of the channel; by increasing the *SVF* from 1% to 4% the dimensionless velocity is reduced by 0.16 in the corrugated area and remains nearly unchanged in the smooth area. The higher effect of *NP* increment on decreasing the axial velocity in the corrugated zone is discussed as the effect of vortices and therefore, the higher effect of fluid viscosity on velocity reduction
- The improving effect of using *NF* is more significant where the effect of other enhancing factors (such as the *Re* number or *SVF* increment) is weak. For wall amplitude of 0.1 m, by increasing the *SVF* from 1 to 4 % the Nu_{avg} increased by 35 % and 22 % in *Re* =8000 and 40,000, respectively.

CRediT authorship contribution statement

Mohammad N. Fares: Formal analysis, Data curation, Conceptualization, Supervision. **Mohammad AL-Saad:** Formal analysis, Writing – original draft. **Heider H.J. Almutter:** Writing – original draft, Writing – review & editing. **Dheyaa J. Jasim:** Data curation, Formal analysis, Validation. **Mohammad Ali Fazilati:** Conceptualization, Data curation, Formal analysis, Supervision, Writing – original draft, Writing – review & editing. **Soheil Salahshour:** Writing – original draft. **Sh. Baghaei:** Formal analysis, Data curation, Conceptualization.

Declaration of competing interest

The authors declare that they have no known competing financial interests or personal relationships that could have appeared to influence the work reported in this paper.

Data availability

No data was used for the research described in the article.

References

[1] R. Fares, F. Mebarek-Oudina, A. Aissa, S. Bilal, H.F. Öztop, Optimal entropy generation in Darcy-Forchheimer magnetized flow in a square enclosure filled with silver based water nanoliquid, J. Therm. Anal. Calorim. (2021) 1–11. Vol.

[2] B. Li, C. Byon, Experimental and numerical study on the heat sink with radial fins and a concentric ring subject to natural convection, Appl. Therm. Eng. 90 (2015) 345–351.

[3] P. Singh, A.K. Patil, Experimental investigation of heat transfer enhancement through embossed fin heat sink under natural convection, Exp. Therm. Fluid. Sci. 61 (2015) 24–33.

[4] M. Lee, H.J. Kim, D.-K. Kim, Nusselt number correlation for natural convection from vertical cylinders with triangular fins, Appl. Therm. Eng. 93 (2016) 1238–1247.

[5] C. Dong, Y.-P. Chen, J.-F. Wu, Flow and heat transfer performances of helical baffle heat exchangers with different baffle configurations, Appl. Therm. Eng. 80 (2015) 328–338.

[6] T. Stamboul, M.A. Saada, A. Campo, Maximum heat transfer reduction in a horizontal porous annular cavity induced by the attachment of symmetric radial baffles to the hot inner cylinder, Appl. Therm. Eng. 93 (2016) 1105–1113.

[7] Y. You, Y. Chen, M. Xie, X. Luo, L. Jiao, S. Huang, Numerical simulation and performance improvement for a small size shell-and-tube heat exchanger with trefoil-hole baffles, Appl. Therm. Eng. 89 (2015) 220–228.

[8] M. Khoshvaght-Aliabadi, O. Sartipzadeh, A. Alizadeh, An experimental study on vortex-generator insert with different arrangements of delta-winglets, Energy 82 (2015) 629–639.

[9] L. Gao, H. Zhang, Y. Liu, S. Han, Effects of vortex generators on a blunt trailing-edge airfoil for wind turbines, Renew. Energy 76 (2015) 303–311.

[10] G. Zhou, M. Pang, Experimental investigations on thermal performance of phase change material–Trombe wall system enhanced by delta winglet vortex generators, Energy 93 (2015) 758–769.

[11] L.O. Salviano, D.J. Dezan, J.I. Yanagihara, Thermal-hydraulic performance optimization of inline and staggered fin-tube compact heat exchangers applying longitudinal vortex generators, Appl. Therm. Eng. 95 (2016) 311–329.

[12] M. Sheikholeslami, M. Jafaryar, Z. Said, A.I. Alsabery, H. Babazadeh, A. Shafee, Modification for helical turbulator to augment heat transfer behavior of nanomaterial via numerical approach, Appl. Therm. Eng. 182 (2021) 115935.

[13] L. Chen, M. Jafaryar, A. Shafee, R.N. Dara, I. Tlili, Z. Li, Effect of complex turbulator on heat transfer of nanomaterial considering turbulent flow, Microsyst. Technol. 26 (2020) 739–749.

[14] A. Baïri, Using nanofluid saturated porous media to enhance free convective heat transfer around a spherical electronic device, Chin. J. Phys. 70 (2021) 106–116.

[15] P. Talebizadeh Sardari, G.S. Walker, M. Gillott, D. Grant, D. Giddings, Numerical modelling of phase change material melting process embedded in porous media: effect of heat storage size, in: Proceedings of the institution of mechanical engineers, Part A: journal of power and energy 234, 2020, pp. 365–383.

[16] P.K. Chaurasiya, S.K. Singh, P.K. Jain, U. Rajak, T.N. Verma, A. Azad, K. Choudhary, A.M. Alosaimi, A. Khan, Heat transfer and friction factor correlations for double pipe heat exchanger with inner and outer corrugation, Energy Sources A: Recovery Util. Environ. Eff. (2021) 1–28. Vol.

[17] P. Dutta, P.P. Dutta, P. Kalita, P. Goswami, P.K. Choudhury, Energy analysis of a mixed-mode corrugated aluminium alloy (AlMn1Cu) plate solar air heater, Mater. Today: Proc. (2021). Vol..

[18] G.G. Cruz, M.A. Mendes, J.M. Pereira, H. Santos, A. Nikulin, A.S. Moita, Experimental and numerical characterization of single-phase pressure drop and heat transfer enhancement in helical corrugated tubes, Int. J. Heat. Mass Transf. 179 (2021) 121632.

[19] M. Siavashi, M. Jamali, Heat transfer and entropy generation analysis of turbulent flow of TiO2-water nanofluid inside annuli with different radius ratios using two-phase mixture model, Appl. Therm. Eng. 100 (2016) 1149–1160.

[20] M. Siddique, A.-R. Khaled, N. Abdulhafiz, A. Boukhary, Recent advances in heat transfer enhancements: a review report, Int. J. Chemical Eng. 2010 (2010).

[21] L.S. Ismail, R. Velraj, C. Ranganayakulu, Studies on pumping power in terms of pressure drop and heat transfer characteristics of compact plate-fin heat exchangers—A review, Renew. Sustain. Energy Rev. 14 (2010) 478–485.

[22] A. Shenoy, M. Sheremet, I. Pop, Convective Flow and Heat Transfer from Wavy surfaces: Viscous fluids, Porous media, and Nanofluids, CRC press, 2016.

[23] S.M. Vanaki, H. Mohammed, A. Abdollahi, M. Wahid, Effect of nanoparticle shapes on the heat transfer enhancement in a wavy channel with different phase shifts, J. Mol. Liq. 196 (2014) 32–42.

[24] M. Ahmed, N. Shuaib, M.Z. Yusoff, A. Al-Falahi, Numerical investigations of flow and heat transfer enhancement in a corrugated channel using nanofluid, Int. Commun. Heat Mass Transf. 38 (2011) 1368–1375.

[25] M. Akbarzadeh, S. Rashidi, M. Bovand, R. Ellahi, A sensitivity analysis on thermal and pumping power for the flow of nanofluid inside a wavy channel, J. Mol. Liq. 220 (2016) 1–13.

[26] Y. Sui, C. Teo, P. Lee, Direct numerical simulation of fluid flow and heat transfer in periodic wavy channels with rectangular cross-sections, Int. J. Heat. Mass Transf. 55 (2012) 73–88.

[27] D. Ferley, S. Ormiston, Numerical analysis of laminar forced convection in corrugated-plate channels with sinusoidal, ellipse, and rounded-vee wall shapes, Numer. Heat Transf.; A: Appl. 63 (2013) 563–589.

[28] Zare, H., Banooni, S., and Ghanbarzadeh, A., "Optimal design of plate-fin heat exchangers by a bees algorithm", Vol., 2013.

[29] S.K. Mehta, S. Pati, L. Baranyi, Effect of amplitude of walls on thermal and hydrodynamic characteristics of laminar flow through an asymmetric wavy channel, Case Stud. Therm. Eng. 31 (2022) 101796.

[30] F. Selimefendigil, H.F. Öztop, Thermal management and performance improvement by using coupled effects of magnetic field and phase change material for hybrid nanoliquid convection through a 3D vented cylindrical cavity, Int. J. Heat. Mass Transf. 183 (2022) 122233.

[31] F. Selimefendigil, H.F. Öztop, Thermal management for conjugate heat transfer of curved solid conductive panel coupled with different cooling systems using non-Newtonian power law nanofluid applicable to photovoltaic panel systems, Int. J. Therm. Sci. 173 (2022) 107390.

[32] M. Gupta, N. Arora, R. Kumar, S. Kumar, N. Dilbaghi, A comprehensive review of experimental investigations of forced convective heat transfer characteristics for various nanofluids, Int. J. Mech. Mater. Eng. 9 (2014) 1–21.

[33] A.M. Hussein, K. Sharma, R. Bakar, K. Kadirgama, A review of forced convection heat transfer enhancement and hydrodynamic characteristics of a nanofluid, Renew. Sustain. Energy Rev. 29 (2014) 734–743.

[34] M. Rashidi, A. Hosseini, I. Pop, S. Kumar, N. Freidoonimehr, Comparative numerical study of single and two-phase models of nanofluid heat transfer in wavy channel, Appl. Math. Mech. 35 (2014) 831–848.

[35] S. Göktepe, K. Atalık, H. Ertürk, Comparison of single and two-phase models for nanofluid convection at the entrance of a uniformly heated tube, Int. J. Therm. Sci. 80 (2014) 83–92.

[36] M. Hejazian, M.K. Moraveji, A. Beheshti, Comparative numerical investigation on TiO2/water nanofluid turbulent flow by implementation of single phase and two phase approaches, Numer. Heat Transf.; A: Appl. 66 (2014) 330–348.

[37] R. Dormohammadi, M. Farzaneh-Gord, A. Ebrahimi-Moghadam, M.H. Ahmadi, Heat transfer and entropy generation of the nanofluid flow inside sinusoidal wavy channels, J. Mol. Liq. 269 (2018) 229–240.

[38] Kumar, P., and Dwivedi, R., "Thermo-hydraulic transport characteristics of non-Newtonian nanofluid flow through wavy channel: influence of nanoparticle volume fraction and Prandtl number", *Numer. Heat Transf.; A: Appl.*, pp. 1–20, 2024.

[39] M. Hajialibabaei, M.Z. Saghir, I. Dincer, Y. Bicer, Optimization of heat dissipation in novel design wavy channel heat sinks for better performance, Energy 297 (2024) 131155.

[40] Y.A. Cengel, S. Klein, W. Beckman, Heat transfer: a Practical Approach, WBC McGraw-Hill Boston, 1998.
[41] Y.-Q. Song, N. Izadpanahi, M.A. Fazilati, Y.-P. Lv, D. Toghraie, Numerical analysis of flow and heat transfer in an elliptical duct fitted with two rotating twisted tapes, Int. Commun. Heat Mass Transf. 125 (2021) 105328.
[42] S. Rashidi, M. Akbarzadeh, N. Karimi, R. Masoodi, Combined effects of nanofluid and transverse twisted-baffles on the flow structures, heat transfer and irreversibilities inside a square duct–a numerical study, Appl. Therm. Eng. 130 (2018) 135–148.
[43] M. Amani, P. Amani, A. Kasaeian, O. Mahian, W.-M. Yan, Two-phase mixture model for nanofluid turbulent flow and heat transfer: effect of heterogeneous distribution of nanoparticles, Chem. Eng. Sci. 167 (2017) 135–144.
[44] S.A. Manavi, A. Ramiar, A.A. Ranjbar, Turbulent forced convection of nanofluid in a wavy channel using two phase model, Heat and Mass Transfer 50 (2014) 661–671.